# THESIS REPORT

## Master's Degree

## Implementation of a Designed Tool Post for Tool Vibration Compensation Using PMN Actuators

*by H. Luu*
*Advisor: G.M. Zhang*

**M.S. 96 -10**

**ISR**

INSTITUTE FOR SYSTEMS RESEARCH

| Report Documentation Page | | | | _Form Approved_ _OMB No. 0704-0188_ |
|---|---|---|---|---|

Public reporting burden for the collection of information is estimated to average 1 hour per response, including the time for reviewing instructions, searching existing data sources, gathering and maintaining the data needed, and completing and reviewing the collection of information. Send comments regarding this burden estimate or any other aspect of this collection of information, including suggestions for reducing this burden, to Washington Headquarters Services, Directorate for Information Operations and Reports, 1215 Jefferson Davis Highway, Suite 1204, Arlington VA 22202-4302. Respondents should be aware that notwithstanding any other provision of law, no person shall be subject to a penalty for failing to comply with a collection of information if it does not display a currently valid OMB control number.

| 1. REPORT DATE **1996** | 2. REPORT TYPE | 3. DATES COVERED |
|---|---|---|

| 4. TITLE AND SUBTITLE **Implementation of a Designed Tool Post for Tool Vibration Compensation Using PMN Actuators** | 5a. CONTRACT NUMBER |
|---|---|
| | 5b. GRANT NUMBER |
| | 5c. PROGRAM ELEMENT NUMBER |
| 6. AUTHOR(S) | 5d. PROJECT NUMBER |
| | 5e. TASK NUMBER |
| | 5f. WORK UNIT NUMBER |

| 7. PERFORMING ORGANIZATION NAME(S) AND ADDRESS(ES) **University of Maryland,The Graduate School,2123 Lee Building,College Park,MD,20742** | 8. PERFORMING ORGANIZATION REPORT NUMBER |
|---|---|
| 9. SPONSORING/MONITORING AGENCY NAME(S) AND ADDRESS(ES) | 10. SPONSOR/MONITOR'S ACRONYM(S) |
| | 11. SPONSOR/MONITOR'S REPORT NUMBER(S) |

| 12. DISTRIBUTION/AVAILABILITY STATEMENT **Approved for public release; distribution unlimited.** |
|---|

| 13. SUPPLEMENTARY NOTES |
|---|

| 14. ABSTRACT **see report** |
|---|

| 15. SUBJECT TERMS |
|---|

| 16. SECURITY CLASSIFICATION OF: | | | 17. LIMITATION OF ABSTRACT | 18. NUMBER OF PAGES **120** | 19a. NAME OF RESPONSIBLE PERSON |
|---|---|---|---|---|---|
| a. REPORT **unclassified** | b. ABSTRACT **unclassified** | c. THIS PAGE **unclassified** | | | |

**Standard Form 298 (Rev. 8-98)**
Prescribed by ANSI Std Z39-18

# Implementation of a Designed Tool Post for Tool

# Vibration Compensation Using PMN Actuators

by

**Huynh Luu**

Thesis submitted to the Faculty of the Graduate School
of the University of Maryland in partial fulfillment
of the requirements for the degree of
Master of Science
1996

Advisory Committee:

Associate Professor Guangming Zhang, Chairman/Advisor
Assistant Professor Balakumar Balachandran
Professor Andre Tits

# ABSTRACT

| | |
|---|---|
| Title of Thesis: | Implementation of a Designed Tool Post for Tool Vibration Compensation Using PMN Actuators |
| Name of degree candidate: | Huynh Luu |
| Degree and Year: | Master of Science, 1996 |
| Thesis directed by: | Dr. Guangming Zhang, Associate Professor, Department of Mechanical Engineering and Institute for Systems Research |

Tool vibration is a well-known fact in causing poor surface finish, accelerated tool wear, and unstable machining operations. Due to the availability of active or "smart" materials, researchers in the machine tool industry are now focusing on applying active control to attenuate tool vibration during machining.

In this thesis research, efforts are dedicated to investigating the mechanical and electrical behavior of a designed tool post structure in which lead-magnesium-niobate (PMN) actuators are used as built-in devices for vibration control. Research is focused on using finite element method (FEM) to identify the dynamic characteristics of the tool post, establishing an experimental testbed environment for experimental verifications, and implementing the tool post in a shop floor machining environment to test its performance, both mechanically and electronically.

Results obtained from this investigation has justified the tool post design for its effectiveness in carrying out vibration compensation during machining. A 10 to 20 percent of reduction has been observed with the PMN actuators in action. Significant findings of this research include 2 to 3 $\mu$m floating of the dynamic equilibrium position of the tool tip during the compensation, and the effect of interplay between actuator-driving frequency and workpiece rotation on in-process compensation. Control of the coupling coefficient deserves special attention for maintaining an acceptable efficiency of conversion from electrical energy to mechanical energy. Knowledge gained from this study has provided guidelines not only for off-line optimization, but also for controller designs when PMN actuators are applied.

# DEDICATION

To my family,

for all their encouragement and support

# ACKNOWLEDGMENTS

# TABLE OF CONTENTS

**References**                                                                           **103**

# LIST OF TABLES

# LIST OF FIGURES

# Chapter 1

# Introduction

## 1.1   Importance of the Machine Tool Industry

At the turn of the twentieth century, the United States had one of the most dominant national economy in the world.  The most contributing factor that led to this economic leadership was technological development in the industrial sector.  In terms of economics standards, there was a huge technological gap between the United States and the world's next best economies.  Within that time period, technological innovation had helped the U.S. industries in maintaining a steady stream of new and improved products and services to promote economic growth, provided job opportunities, and ensured national security.

However, in the early 1960s, other nations in Europe and Asia began to emerge with their technological prowess and compete with the United States in technological development.  As a result of such competition, the United States began to lose its industrial preeminence and its role as economic leader.  But what is more disturbing is that the United States continues to show a steady decline and thus lose ground to international competitors in world trade as well as in domestic

market [1].

To regain the competitiveness in the tool industry in the United States, a Machine Tool Panel under the support of the National Research Council conducted a study on the role of technological development in determining industrial competitiveness. The study found that at the center of the technological development is the machine tool industry. Although, the machine tool industry is a relatively small industry accounting for only 0.10 percent of the gross national product, the industry is vital. Almost every major manufactured product is built on a machine tool or on a machine made by a machine tool. The performance of the industry in the market place has a direct link to the growth of the overall economy. Any fluctuating activities generated by the industry has shown a ripple or a multiplier effect on income and employment throughout the industrial base.

The study also found that the American industry is starting to lag behind several countries especially in the area of machine software and control units. In order to remain competitive in the global market, the panel suggested Congress to provide assistance to small businesses to promote development of ideas and innovations from conceptualization to application, establish a channel for technical assistance and advisory services to industries particularly small businesses, and grant research supports for industrial innovation, including cooperative industry-university basic and applied research [2].

## 1.2 National Efforts in Regaining Competitiveness

In response to the need of increasing the American industry to regain competitiveness in the marketplace, efforts to promote the machine tool industry in this country have been made. One of these efforts is to apply new and innovative technologies to revolutionize machine tools. The Advanced Research Projects Agency (ARPA) granted supports to the Smart Materials and Structures (SMS) Partnership to conduct innovative research in the area of synthesis and processing of smart materials. This unique partnership consists of managing partners, system integrators, manufacturers, government laboratories, universities, and state and local government. The partners involved in the partnership include the following: Martin Marietta Laboratories, AVX Corporation, Lockheed Missiles and Space Company, BDM Federal, Naval Research Laboratories, Virginia Tech, University of Maryland at College Park, Clemson University, Denver University, and Johns Hopkins University. The main goals of the research efforts are as follows [3].

1. To develop state-of-the-art technology in synthesis and processing of multilayer ceramics actuators (MCA) and shape memory alloy (SMA) actuators to increase availability with low-cost production capability.

2. To broaden the application of electromechanical actuators at the macro-scale and micro-scale levels for structural vibration cancellation.

3. To promote the commercialization of advanced technology through university/industry partnership.

The work presented in this thesis represents part of the University of Maryland's participation in SMS Partnership project. The ultimate goal of the project is to develop a tool post structure in which actuators made from smart materials are used as built-in devices to perform active vibration control. Under this project, a smart tool post structure has been designed and fabricated. A microprocessor-based control system has been built to command the vibration attenuation. The scope of this thesis is to implement the designed tool post structure and the control system from a testbed environment to a machining environment.

## 1.3 Thesis Organization

There are six chapters and three appendices to this thesis. The contents of each chapter are summarized below.

Chapter 1 presents an introduction to the importance of the machine tool industry to the U. S. economy and the national efforts to revive the industry to remain competitive. Part of the national efforts is ARPA's research grant to the SMS Partnerships with the University of Maryland at College Park as one of the

partners. The University of Maryland team is responsible for designing a machine tool post for active vibration control.

In Chapter 2, an overview of the relevant literature starting with the basic operation of a lathe is given. Then, the mechanics of material removal for cutting operation is covered with emphasis on the formation of chips, the interaction of cutting force, and the occurrence of vibration during machining. The chapter concludes with summaries and results from two previous master's theses work.

In Chapter 3, the design analysis using finite element method of the membrane components is presented. The analysis includes the prediction of the membrane stiffness, the statics and dynamics behavior of the membrane, and buckling analysis.

In Chapter 4, the components of an experimental testbed in which the smart tool post was tested including the sensing system, the power amplification system, and the data acquisition system are described. Instrumentation setup and preparation as well as experimental tests are described.

In Chapter 5, the machining tests conducted on the shop floor to evaluate the performance of the smart tool post structure are discussed. A series of design of experimentation was employed to provide a systematic study of the performance of the smart tool post structure and the control system to provide active vibration control in the actual machining operation. Results and discussion of four sets of experiments are presented.

In Chapter 6, conclusions and recommendations for future work are presented.

In Appendix A, the hardware used in the data acquisition system are described including hardware setup and connections. Appendix B contains the coding of the programs written in LabVIEW. The functions of these programs include driving the exciter, collecting data, communicating with the controller circuitry, and manipulating data for analysis. Specifications of the PMN actuators such as the capacitance, the stroke limits, and the response curves are provided in Appendix C. Appendix D contains plots of the experimental data as well as the surface profile measurements of the aluminum workpiece.

# Chapter 2

# Literature Review

## 2.1 Machining and Turning Operations

There are a variety of machine tools available in the market, each designed for a specific industrial application. For instance, milling machine tools are used for making slots for die cavities and producing curved shapes for gears. Grinding machine tools are used to achieve high finish quality and dimensional accuracy, but with relatively low productivity when compared with milling operations. Of all the machine tools, the most popular are lathes. In general, a lathe is a machine tool that rotates the work material while cutting is achieved by moving a single-point cutting tool against the workpiece. In some lathes, however, the cutting tool may rotate while the workpiece remains stationary during machining.

The history of the lathes can be traced back to the screw-cutting engine lathes that are considered as the oldest and most important of machine tools. The earliest record of a screw cutting lathe dates back to the 1740s in France. However it was not until late 1700s that the first practical screw-cutting lathe was built. The

first lathe was slow and clumsy, but its invention had started the history of modern machinery. As a result, the lathe became known as the "King of All Tools." [4]

The main components of a Clausing Colchester 15" lathe are shown in Figure 2-1 below [5]. This is the lathe that is being used in testing the performance of the smart tool post structure. During operation, the chuck which is mounted at the headstock is rotated by the gear train assembly. The workpiece is clamped by the chuck. If the workpiece is long, the tailstock may be used to support the workpiece. The cutting tool is fixed onto the tool post and is mounted on the saddle and the cross slide. The carriage may be moved horizontally along the lathe bed manually or automatically by either disengaging or engaging the power feed screw. The cross feed knob allows the tool post to be moved perpendicularly to the longitudinal feed direction. The top slide gives the flexibility of changing the angle of the cross feed direction [6].

The development of the Computer Numerically Controlled (CNC) machines marked one of the revolutionary developments in the machine tool industry. CNC machining offers several advantages such as improving the uniformity in manufactured products, facilitating contour machining, and adding flexibility to milling and drilling operations. Despite the sophistication of CNC machines, vibration during machining still remains a major issue. In fact, the tool vibration control becomes more critical in quality and productivity improvement when using NC machines.

8

LEGEND

1 Headstock
2 Spindle
3 Topslide
4 Splash guard
5 Tailstock
6 Bed
7 Mounting feet
8 Tail-end plinth
9 Leadscrew
10 Coolant tray
11 Saddle and cross-slide
12 Apron
13 Footbrake
14 Head-end plinth
15 Gearbox
16 End cover (gear train)

Figure 2-1  Main components of a Clausing Colchester 15" lathe

In a machining process, it is well known that the dimensional accuracy of a manufactured part depends on the deflection of the spindle as well as on the accuracy of the relative position between the tool and the workpiece. As a result,

9

the accuracy and the finish quality that a machine can achieve depend on many factors such as the rigidity of the machine tool, the type of cutting tools, and the material of the workpiece. One of the most important parameters to measure accuracy in machining operations is surface finish. Surface finish can be quantified by measuring the surface roughness using stylus instruments in which the surface topography of the machined part is traced by traversing a diamond stylus over the surface. The standard for measuring the surface roughness is the center line average (CLA) value or arithmetic average (AA) or simply Ra where the roughness is obtained by measuring the mean deviation of the peaks from the center line. The center line is defined as the line that divides the surface trace into equal areas above and below the line. Other units of measurement of surface roughness include the root mean square (RMS) and peak-to-valley roughness (PV).

Achieving a good surface finish in machine parts is difficult. In products where surface finish is related to the products' performance such as gears, cam surfaces, and face seals, it has been found that performance varies linearly as the surface roughness varies logarithmically. Quantitatively, for every twofold improvement in performance, there must be at least a tenfold improvement in the surface finish. For turning operation, the range of roughness (Ra) for finish machining is between 30 $\mu$in to 60 $\mu$in (0.75 $\mu$m to 1.5 $\mu$m). But in general, having a surface finish at about 160 $\mu$in (4 $\mu$m) is satisfactory for most applications [7].

## 2.2 Dynamics of Machining Systems

Static and dynamics stability of a machine system has always been an interest to the machine tools research community because during the cutting, the machine structure has an influence in limiting the machine tool performance. The relationship that occurs in turning operation can best be described by Merritt's block diagram as shown in Figure 2-2 below [8].
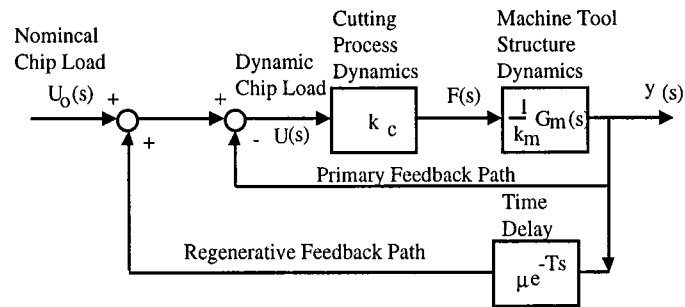


Figure 2-2  Block diagram of a machining system.

As show in the figure above, the machining system consists of three major components: the cutting process dynamics, the machine structure dynamics, and two feedback paths, the primary feedback path and the regenerative feedback path. The dynamics of the cutting process is related to the instantaneous uncut chip thickness and the cutting force generated. Much work had been done on studying the cutting process dynamics, however, experimental confirmations were lacking up to that time period. In Merritt's work, he assumed a steady-state cutting process.

As a result, the cutting process dynamics is neglected.

Unlike the cutting process, the dynamics of the machine structure can be approximated by partial differential equations using lumped-parameter analysis. However, since the resulting cutting force is in space vector, there exists a variety of dynamic responses for each orientation of the cutter and the machine structure. As a result, experimentation must be conducted for each machining conditions to obtain the dynamic characteristics of the machine structure.

In the feedback paths, the primary feedback path is always present. However, the regenerative feedback path may or may not occur depending on the overlap factor. The overlap factor is the condition in which the material from the previous revolution is recut.

## 2.3   Mechanics of Material Removal in Metal Cutting

During turning operation, the workpiece is held in the chuck of the lathe and rotated. Cutting is made as the cutting tool moved horizontally along the axis of the bar at a constant speed. The cutting speed (V) is the rate that the uncut surface of the workpiece passes the cutting edge of the tool. The unit of the cutting speed is expressed in ft/min or m/min. The feed (f) with unit in in/rev or mm/rev is the distance the tool moves along the axis of the workpiece at each revolution of the work material. The depth of cut (d) is the thickness of the metal removed from the

12

workpiece which can be expressed in inches or mm. During a cutting operation, the efficiency of metal removed is often measured in terms of the rate of metal removal which can be expressed as the product of the cutting speed, the feed rate, and the depth of cut.

## 2.3.1 Chip Formation during Machining

One of the most important aspects of metal cutting is the interaction between the cutting tool and the workpiece in the formation of chip. The classical theory of chip formation has been based on Merchant's theory of metal cutting. In his theory, Merchant proposed that the formation of chip is a steady process in which the chip is produced continuously and uniformly by the shearing action along the shearing plane of the workpiece material. Since the chip is produced in plane strain, the width of the chip is equal to the undeformed chip width. The frictional forces developed between the workpiece surface and the cutting tool surface are sufficient to restrain the movement of the workpiece surface across the tool surface. As a result, the chip is formed due to the frictional restraint.

In general, orthogonal cutting operation gives a good approximation to describe the performance of the majority of cutting edges since the chip formed during cutting is assumed to be continuous. Orthogonal cutting describes the condition when the chip is formed in two-dimension with the chip flow in a direction

perpendicular to the cutting edge. During metal cutting, the metal is sheared off along the shear plane as shown in the figure below [9].
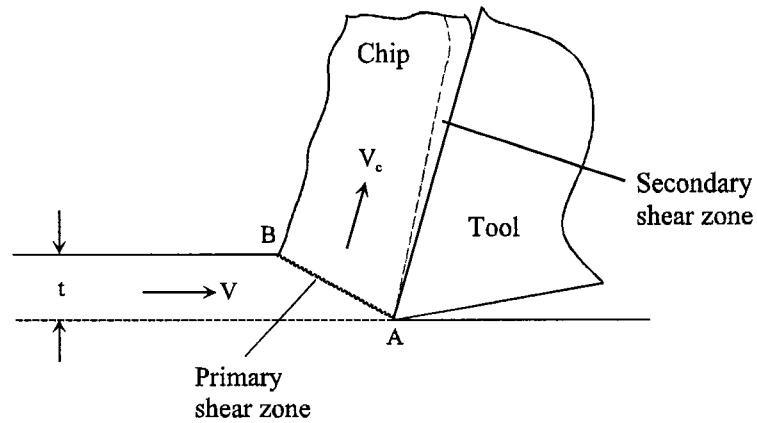


Figure 2-3  Production of chip at the shear plane

## 2.3.2  Built-up Edge Effect

During the formation of chip, chip fracture may develop due to the relatively low temperature at the tool-chip interface. Strain hardening occurs on the chip material resulting in portion of the chip being attached to the tool surface. This condition is known as built-up edge (BUE). Figure 2-4 shows the effect of BUE on the tool tip. One of the major effects of BUE is to cause poor surface finish as shown in Figure 2-5. However, BUE is avoidable. In general, for typical turning conditions a large BUE value is obtained when the cutting speed is at about 10 in/s (0.3 m/s) and disappears at 40 in/s (1.2 m/s) [10].

14
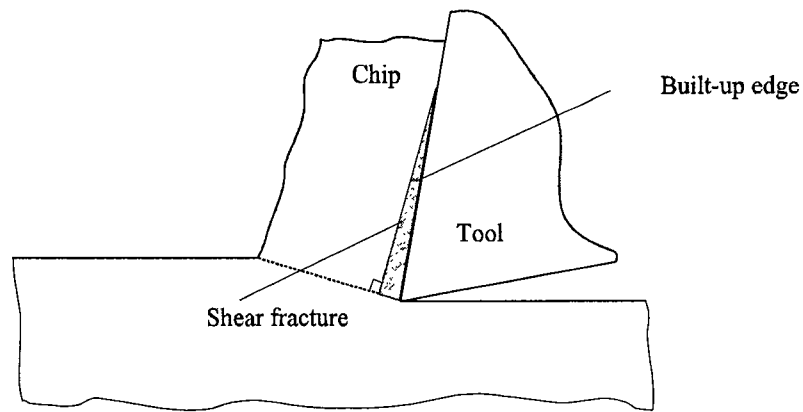
Figure 2-4  Built-up edge effect at the tool-chip interface
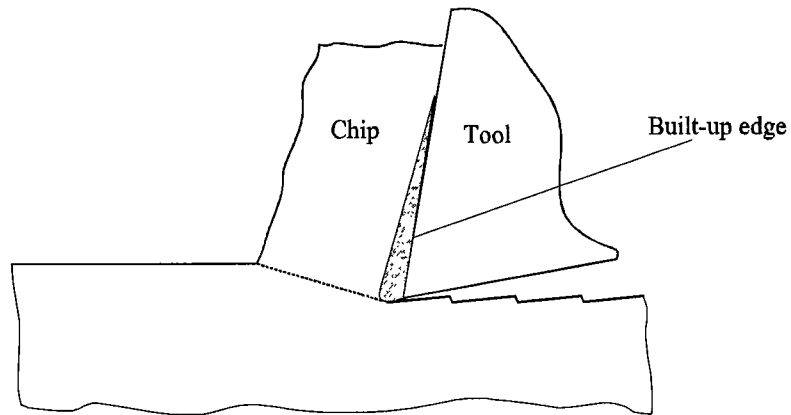


Figure 2-5  Effect of built-up edge on surface roughness

### 2.3.3 Cutting Force in Turning Operation

In a turning operation, the force components can be measured as shown in Figure 2-6 below.  The force component acting normal to the cutting edge of the tool in the direction $YO$ is the cutting force, $F_C$.  This force component is usually the largest of the three force components.  The force component acting along the feed

direction, or along the axis of the workpiece in the *OX* is the feed force, $F_f$. The third force component acting in the *OZ* direction is the radial force, $F_r$. During machining, the radial force pushes the cutting tip away from the workpiece. Of the three force components, the radial force components is usually the smallest. In general, the forces involved in machining are relatively small. The layer of metal removed such as the chip is thin. As a result, the force is usually of no more than a few hundreds Newtons.
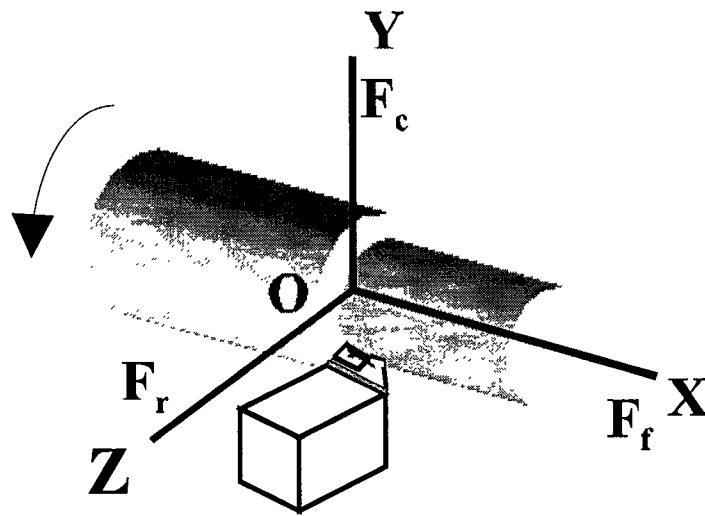


Figure 2-6 Three components of the cutting force in turning operation

From the chip formation viewpoint, the two most important force interactions are the interaction between the tool surface and the chip denoted as R, and the interaction between the workpiece and the chip denoted as R'. Under static equilibrium, these two force interactions must be equal. From a free body diagram,

16

the sets of force components of the chip formed are as shown in Figure 2-7 [11].
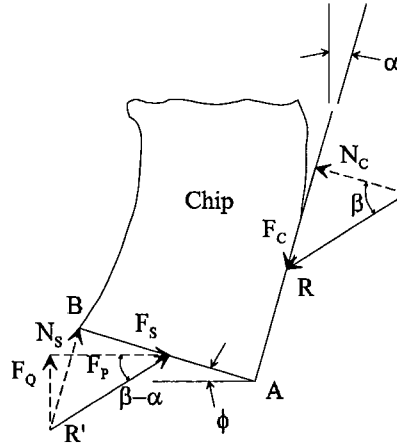
Figure 2-7  Free body diagram showing the force components on a chip

Based on Merchant's cutting force diagram as shown in Figure 2-8, the relationship between R and R' can be expressed in terms of the shear and friction components of force ($F_p$ and $F_q$).
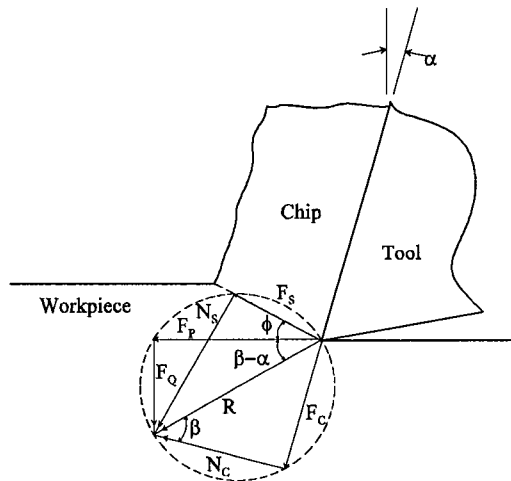
Figure 2-8  Merchant's cutting force circle

17

(a) Shear plane         (b) Tool surface
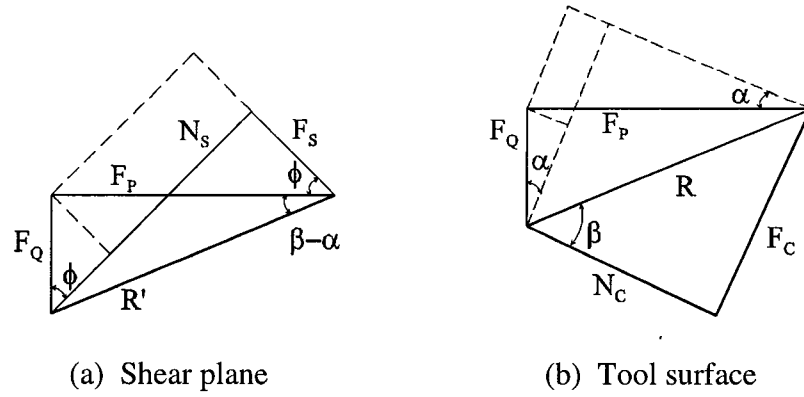
Figure 2-9 Geometrical derivation of the resultant force

From Figure 2-9a above,

$$F_S = F_P \cos\phi - F_Q \sin\phi \tag{2-1}$$

$$N_S = F_Q \cos\phi + F_P \sin\phi = F_S \tan(\phi + \beta - \alpha) \tag{2-2}$$

From equations 2-1 and 2-2, the shear and normal stress can be determined

since

$$\tau = \frac{F_S}{A_S} \tag{2-3}$$

$$A_S = \frac{bt}{\sin\phi} \tag{2-4}$$

where b is the width of the chip and t is the depth of cut.

Combining equations 2-1 through 2-4,

18

$$\tau = \frac{F_S}{A_S} = \frac{(F_P \cos\phi - F_Q \sin\phi)\sin\phi}{bt} \qquad (2\text{-}5)$$

$$\sigma = \frac{N_S}{A_S} = \frac{(FP\sin\phi + FQ\cos\phi)\sin\phi}{bt} \qquad (2\text{-}6)$$

Similarly, from Figure 2-9b,

$$F_C = F_P \sin\alpha + F_Q \cos\alpha \qquad (2\text{-}7)$$

$$N_C = F_P \cos\alpha - F_Q \sin\alpha \qquad (2\text{-}8)$$

Combining equations 2-7 and 2-8 gives the coefficient of friction on the tool

surface as

$$\mu = \frac{F_C}{N_C} = \frac{F_P \sin\alpha + F_Q \cos\alpha}{F_P \cos\alpha - F_Q \sin\alpha} = \frac{F_Q + F_P \tan\alpha}{F_P - F_Q \tan\alpha} \qquad (2\text{-}9)$$

As a result, the frictional force between the cutting tool surface and the

workpiece in the formation of chips can be determined. The cutting force, however,

has its dynamic variation in nature. Such variation depends on the tool geometry,

material being machined, and the cutting conditions. It has been found that in the

frequency domain, the force frequencies are between 20 Hz and 200 Hz [12].

## 2.4 Vibration in Machining System

There are several causes that lead to tool vibration during machining. These causes can be classified as external excitation and self-excitation. Examples of external excitations are foundation excitation due to unsymmetrical rotor alignment and clearance excitation in gears and bearings. The vibration from external excitations is relatively easy to find and isolate. On the other hand, self-excitation during the machining process may not be so easy to identify and isolate. This self-excited vibration is often referred to as chatter. Chatter is inherent in almost all machining conditions since it is the results of the feedback in the machine tool during the cutting process. Chatter may occur when the fluctuation in time of the shearing action between the cutting tip and the workpiece coincides with the natural vibration period of the tool, the tool holder, or the workpiece [13].

There are three classes of chatter: negative damping chatter (or Arnold-type chatter), mode coupling chatter, and regenerative chatter. Arnold-type chatter is caused by the variation of force due to changes with respect to the cutting speed. Mode coupling, on the other hand, is caused by the excitation generated by the elliptical path in which the tool tip displaces. Along this path, energy is input into the system that either excites or compensates the vibrations. As for the regenerative chatter, the self-excited vibration are caused due to re-cutting of the modulating surfaces from previous revolution [14].

### 2.4.1 Vibration Control

To control the vibration of the machine tools and thus improve the surface quality of the finished product, extensive research has been conducted to reconsider the design criteria of the machine tools, such as changing the overall stiffness of a machine tool, increasing the effective mass of the machine, and using low-coefficient-of-thermal expansion materials for gears and bearings. However, it has been found that many design changes made during the past represent a compromise to balance the need to improve the dynamic behavior of a machine system with the cost to pay for these changes. The cost usually is so high that hardware realization of these changes has been slow. As a result, further improvement with cost effectiveness has been an on-going challenge facing the machine tool industry and its research community [15].

### 2.4.2 Application of Active Elements for Vibration Control

With the rapid development of smart material that results in lower production cost and higher performance, the availability of smart material as built-in electromechanical devices offers an attractive opportunity to introduce active elements into the machine tools industry. In particular, the key area that can fully utilize such built-in devices is in the control system. Active elements can be

21

implemented to a control system to be used as either actuating or sensing elements. As an intelligent system, it can adapt to its environment. As a result, the system can yield higher performance and be able to use its resources more efficiently.

In introducing active elements to the machining communities, many factors should be considered to ensure the success of the adaptation: availability of suitable actuators, mathematical modeling of the mechanical systems, appropriate location for actuators and sensors to provide controllability and observability, and integration of system components in terms of hardware and software.

At the current level of technology, the availability of active elements is improving at a rapid pace. Examples of active elements used are magnetic actuators, active chamber system, active tilting pad journal bearings, and piezoelectric actuators. The advantages and disadvantages of each of these active elements are described as follows. There are two types of magnetic actuators, magnetic bearings and electromagnetic actuators. Magnetic bearings impose a magnetic force directly onto the rotor. As a result, the force acts on the rotor without direct physical contact. Electromagnetic actuators on the other hand use bearings to apply the force to the rotor. Current-control loop is generally used in this type of actuators. However, this type of actuators usually requires a large working volume with a relatively small force magnitude.

An active chamber system such as a hydraulic system overcomes the disadvantages of magnetic bearings and electromagnetic actuators with its

compactness and large force magnitude. However, the operating system of hydraulic loops is usually less than 100 Hz. Additionally, hydraulic systems often suffer from leakage problems. Active tilting pad journal bearing, on the other hand, has no moving mechanical parts. However, it has a relatively small region of stability [16].

The advances of ceramic materials has led to the development of ceramic actuators such as piezoelectric actuators or PZT. But, the high hysteresis effect and the stability of PZT pose some limitation its application. As a result, a new generation of smart material known as electrostrictive actuators made from lead-magnesium-niobate or PMN was developed to overcome the problems of PZT actuators. Currently, PMN actuators have low hysteresis problem as well having a wider operating frequency bandwidth.

## 2.5  Current Status of the Smart Tool Post Project

In the duration of the Smart Tool Post Project undertaken by the University of Maryland at College Park, two master theses have been produced in that time period: Ko's thesis work [17]and Dold's thesis work [18]. A summary of their work is described below.

In Ko's thesis, the design of the smart tool post structure is covered from the formulation of the design concept to the fabrication of the tool post structure to the

characterization of several key mechanical components of the structure. In addition, the thesis developed and evaluated a simulation model of a machining system with the smart tool post structure acting as a subsystem. The mechanical components of the smart tool post structure are shown in Figure 2-10.



(a)                                    (b)
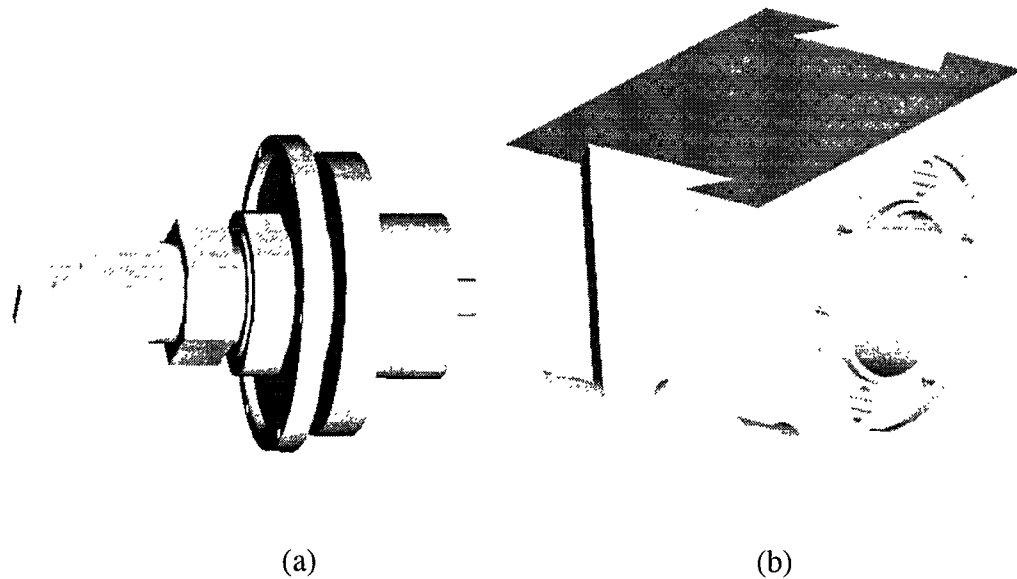
Figure 2-10 The designed smart tool post structure

As shown above, the smart tool post structure consists of a housing unit in which the tool arm is suspended within the housing by two membrane structures. The membrane structures are simply annular rings with constant thickness. At the front of the housing is the cutting tip with a slot for attaching carbide inserts. At the rear of the housing, either a displacement sensor or an accelerometer is mounted to monitor the vibration. Additionally, there are six holes symmetrically located to place the actuators for vibration compensation. The side slots on the outside of the

housing allows the smart tool post to be mounted directly onto the Colchester Lathe.

In Dold's thesis, a control system architecture comprising of a closed feedback loop involving a machining process, a variable-impedance transducer, a microprocessor-based control circuit, and PMN actuators is described. The main components of the control system consist of a sensing element, a phase-shift manipulator, and a self-tuning gain adapter.

The work presented in this thesis shows the continuing efforts to carry the project towards the next stage of completion. The accomplishments of this thesis include the development of an experimental testbed to evaluate the performance of key components of the tool post system such as the sensors, the controller, and the driving mechanisms of the PMN actuators, the introduction of the hardware and software of data acquisition system to collect data as well as analyze data, and the implementation of the tool post in a shop floor machining environment.

# Chapter 3

# Design Analysis Using Finite Element Method

## 3.1 Needs for a Design Analysis

During the last decade, there is a growing trend in adopting rapid prototyping in the product development process [19]. Physical models are built and tested for justification purposes to ensure that the design parameters selected best fit functional needs of the product. However, prototyping may become costly if the associated redesign process is repeated again and again. Determination of the design parameters at an early stage of the design cycle is critical to a cost-effective product development cycle. Therefore, computer-aided engineering has its unique role in providing a virtual environment for design evaluation. In this thesis research finite element method (FEM) is introduced.

Finite element method (FEM) has become a widely used tool during the design cycle. In this thesis, the tool post design is taken as an example to illustrate how FEM can be used to study the static and dynamic behavior of the membrane components of the smart tool post.

## 3.2 Application of FEM into the Tool Post Design

During the design cycle of the smart tool post structure, many studies were conducted using FEM to investigate the characteristic behavior of the membrane components. The studies included the determination of the stiffness of the membrane structure based on various dimensional changes, the deflection of the annular, constant thickness membrane component, and the buckling analysis of the membrane structure. Wherever possible, FEM analyses were compared with experimental results.

### 3.2.1 Prediction of Membrane Stiffness Using FEM

During the design process of the smart tool post structure, determining the geometry and the dimension of the membrane components for the tool post structure was one of the main problems. There were many choices of geometry and dimensions to choose from. As a result, a finite element method was used to predict the stiffness of the membrane based on its geometry and dimension. Figure 3-1 shows a typical geometry of the membrane component. Eight different models with such geometry were built and analyzed using P3/FEA PATRAN 3.0. The dimensions of the geometry used in the finite element analyses are listed in Table 3-1 where H is the height of the shoulder, T is the thickness, and R is the fillet radius.

27
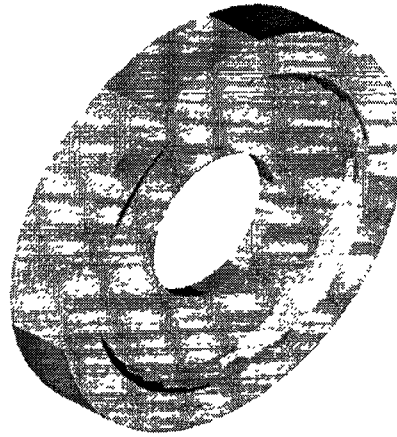
Figure 3-1  Membrane component for the smart tool post structure

Table 3-1  Dimensions of the finite element model

| OD = 2.8 in (71 mm) ID = 1 in (25.4 mm) | | | |
|---|---|---|---|
| Test | H (in) | T (in) | R (in) |
| 1 | 0.28 (7 mm) | 0.12 (3 mm) | 0.08 (2 mm) |
| 2 | 0.28 (7 mm) | 0.12 (3 mm) | 0.04 (1 mm) |
| 3 | 0.28 (7 mm) | 0.08 (2 mm) | 0.08 (2 mm) |
| 4 | 0.28 (7 mm) | 0.08 (2 mm) | 0.04 (1 mm) |
| 5 | 0.20 (7 mm) | 0.12 (3 mm) | 0.08 (2 mm) |
| 6 | 0.20 (7 mm) | 0.12 (3 mm) | 0.04 (1 mm) |
| 7 | 0.20 (7 mm) | 0.08 (2 mm) | 0.08 (2 mm) |
| 8 | 0.20 (7 mm) | 0.08 (2 mm) | 0.04 (1 mm) |

The membrane was modeled as a three-dimensional solid.  Since the geometry is symmetric in the axial direction, only a quarter of the model was built for the analysis as shown in Figure 3-2.  Each of the models was meshed with 560, 8-noded brick elements.
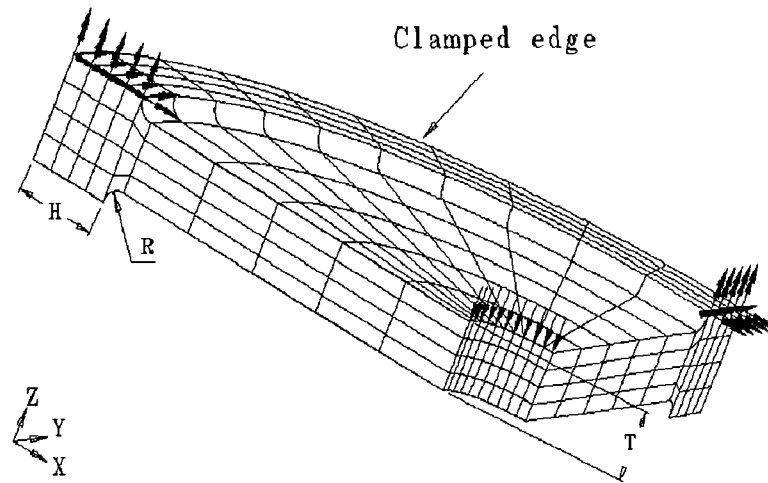
Figure 3-2 Finite element model of the membrane component

In applying the boundary conditions, the outer rim of the model was constrained in the x-, y-, and z-direction. Along the vertical and horizontal faces, where the geometry was sectioned to create the quarter model, they were constrained from moving in the x- and y-direction, respectively. As for the inner rim of the model, a unit force field was evenly distributed among the nodes. The material of the membrane was steel having a Young's modulus of 30 Mpsi (210 GPa) and a Poisson's ratio of 0.3.

With the boundary conditions applied, each of the models was subjected to a linear, static analysis. The result from the calculation is summarized below. From each of the analyses, the stiffness of the membrane was calculated from the following relation.

29

$$F = kx \qquad\qquad (3\text{-}1)$$

where F is the applied unit force in the axial direction

k is the stiffness of the membrane

x is the displacement of the membrane due to the applied

unit force in the axial direction.

Table 3-2 Deformation and stiffness prediction from FEM analyses

| Test | Deformation (in) | Stiffness (lb/in) |
|---|---|---|
| 1 | 0.003 (69.0 μm) | 8.24E4 (1.45E7 N/m) |
| 2 | 0.002 (47.8 μm) | 7.64E4 (1.34E7 N/m) |
| 3 | 0.008 (215.0 μm) | 2.66E4 (4.66E6 N/m) |
| 4 | 0.009 (237.0 μm) | 2.41E4 (4.22E6 N/m) |
| 5 | 0.004 (90.1 μm) | 6.34E4 (1.11E7 N/m) |
| 6 | 0.004 (96.7 μm) | 5.90E4 (1.03E7 N/m) |
| 7 | 0.011 (284.0 μm) | 2.01E4 (3.52E6 N/m) |
| 8 | 0.012 (310.0 μm) | 1.84E4 (3.23E6 N/m) |

With the result of the membrane stiffness obtained from finite element method, a particular set of dimensions for the membrane can be selectively chosen to conduct experimental tests that would yield a stiffness value within the required working range of the tool post design.

### 3.2.2 Geometrical and Dimensional Selection of the Membrane

The final geometry and dimension of the membrane components are shown

in the figure below. As seen in the figure, the membrane is simply an annular ring

with constant cross section. The membrane has an outer diameter of 2.8 in (71.1

mm), an inner diameter of 1 in (25.4 mm), and a constant thickness of 0.12 in (3

mm).
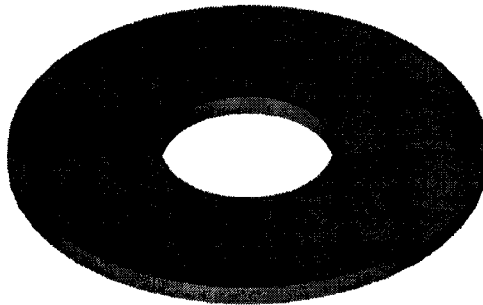
Figure 3-3 The selected geometry of the membrane component
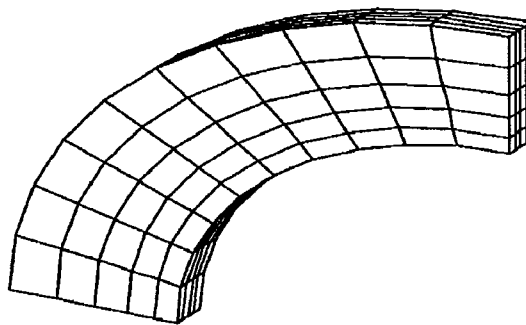
Figure 3-4 FEM meshing model of the membrane component

Similar to previous analysis, finite element method was also used to

determine the stiffness and deflection of the membrane. Since the geometry is

symmetrical, only a quarter of the membrane was modeled for analysis. The FEM

model is shown in Figure 3-4.

The boundary conditions and the material property of the membrane component were applied in the same manner as in the previous analysis. As with any computer prediction, the result needs to be verified. Therefore, an experimental setup was conducted to determine the actual stiffness of the physical membrane component. The experimental setup consisted of a membrane fixture, a Fotonic measurement system, weights, and signal conditioning units. Details of the experimental setup can be found in Ko's thesis. In the experiment, weight was incrementally added to the membrane. The deflection due to the weight was measured by the Fotonic system. Results from the experiment and the FEM analysis are summarized in the table below. The displacement mode of the membrane can be found in Figure 3-5.

Table 3-3  Results from experiment and FEM analysis

| Experimental Deflection: | 9.8 μin (0.25 μm) |
| FEM Deflection: | 7.5 μin (0.19 μm) |
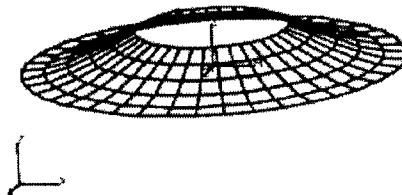


Figure 3-5  Displacement mode of the membrane component

### 3.2.3 Buckling Analysis of the Membrane Component

During the experimental testing of the membrane components, there were concerns about the buckling behavior of the components. As a result, a buckling analysis was conducted. The membrane was modeled as an annular disk with 200, 2-D shell elements. Figure 3-6a and Figure 3-6b show the two different loading conditions used in the analyses. The nodes along the outer edge of the membrane model were fixed in six degrees of freedom. The results of the analyses are shown in Table 3-4.



(a)                                    (b)
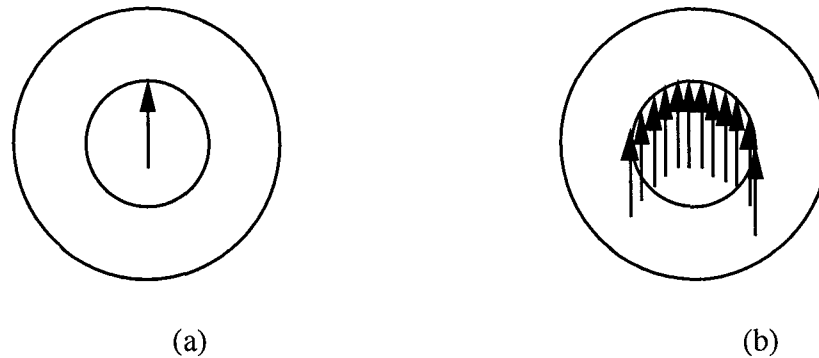
Figure 3-6  Two loading conditions for the buckling analyses

Table 3-4  FEM buckling analysis of the membrane structure.

| Case Description | Critical Load |
|---|---|
| Evenly distributed load | 45.4E3 lbf (202 kN) |
| Single load | 17.2E3 lbf (76.5 kN) |

Based on the results from FEM analysis on the two loading conditions of the 0.024 in (0.61 mm) membrane, the critical buckling load is relatively high for

machining environment. Table 3-5 below shows an example of the cutting force

measurement for a low carbon steel material (pure iron) at a high cutting speed and

large depth of cut using a normal cutting tool with the shear angle at 8°. As can be

seen from Table 3-4 and 3-5, the buckling load of the membrane component is well

above the cutting force in an actual machining environment. Therefore, the

membrane is not likely to buckle during the machining process [20].

Table 3-5  An example of the cutting force measurement of low carbon steel.

| Type of Force | Load Measured |
|---|---|
| Cutting Force, $F_c$ | 315 lbf (1.4 kN) |
| Feed Force, $F_f$ | 270 lbf (1.2 kN) |

# Chapter 4

# Experimental Testbed Environment

## 4.1    Formulation of an Experimental Testbed

In an experimental testbed environment, each component of the machining system is tested. The main advantage of analyzing the system behavior in the testbed environment is the ability to control the settings. Detailed analysis can be made to study the system behavior by altering various parameters within the testbed environment.

As shown in Chapter 2, a closed-loop machining system composes of three major components: the cutting process, the structural dynamics, and the set of feedback paths. Based on Merritt's block diagram of such machining system, a testbed environment is formulated to incorporate the unique features of the smart tool post structure for active vibration control.

Figure 4-1 shows a machining process that has been subdivided into three major subsystems: the machining subsystem, the actuators and control subsystem, and the sensing subsystem. Merritt's closed-loop machining process is grouped into the machining subsystem in which the interaction between the tool and the

35

workpiece can be observed by the output of the tool displacement. In the testbed environment, the tool displacement is observed by the sensing subsystem with sensors such as accelerometers and variable-impedance-transducers (VIT) mounted on the smart tool post structure. The feedback paths and the machining dynamics process of the machining subsystem are information given by the sensors when the tool post structure vibrates. Through a controller in the actuator and controller subsystem, the amplitude and phase of the tool displacement generates the requirement for active vibration control.
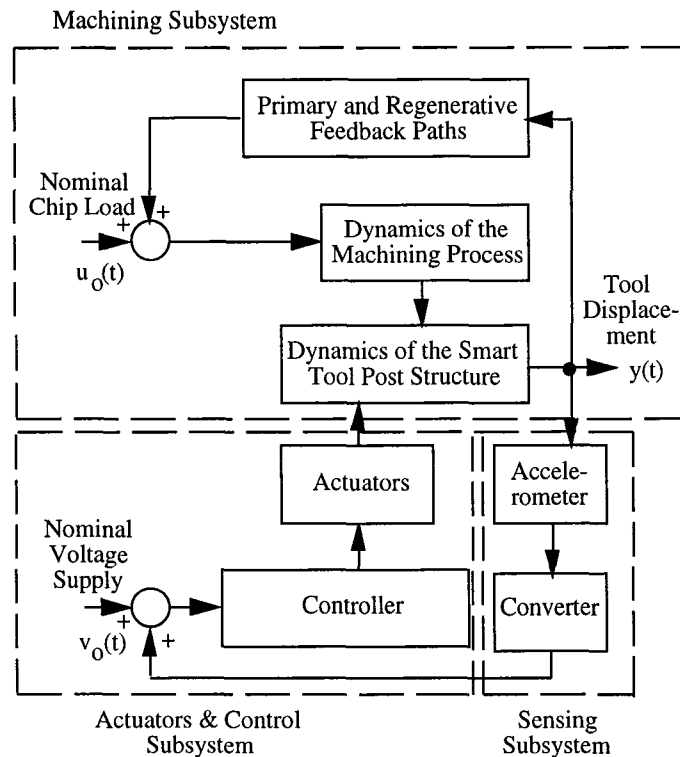
Figure 4-1  Formulation of a machining environment

### 4.1.1 Development of the Testbed

An overview schematic of the finalized testbed and the equipment used during experimentation is shown in Figure 4-2. The testbed consists of a vibration exciter, a load cell to monitor the force exerted by the exciter, a variable-impedance displacement transducer, and the smart tool post structure. All of these components are mounted on a 3"x28"x15" (76x711x381 mm) aluminum plate. Underneath the aluminum plate, a one-inch thick foam pad is used to isolate the aluminum plate and its surrounding. Detailed drawings of the components and the spatial arrangement of the testbed setup are shown in Figure 4-3.
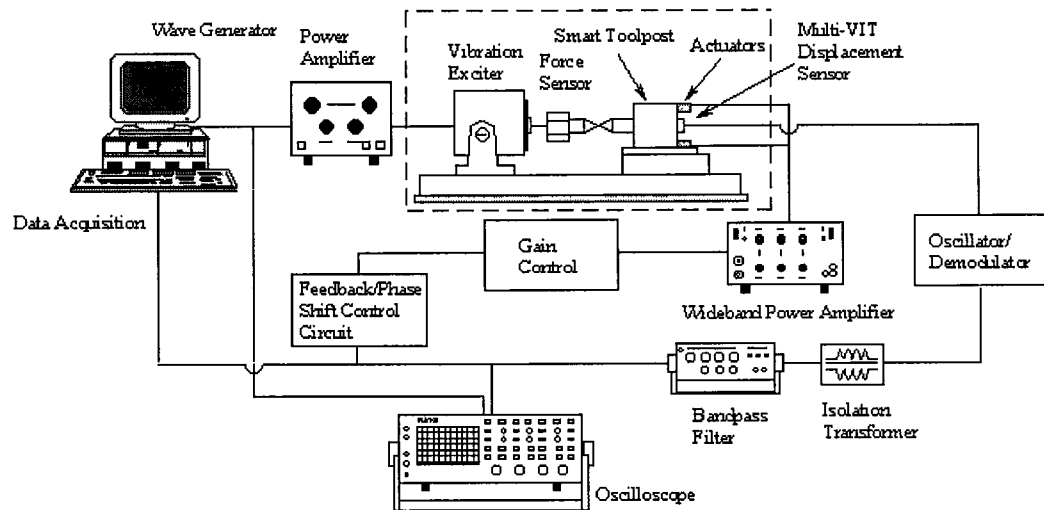
Figure 4-2 Testbed for experimentation
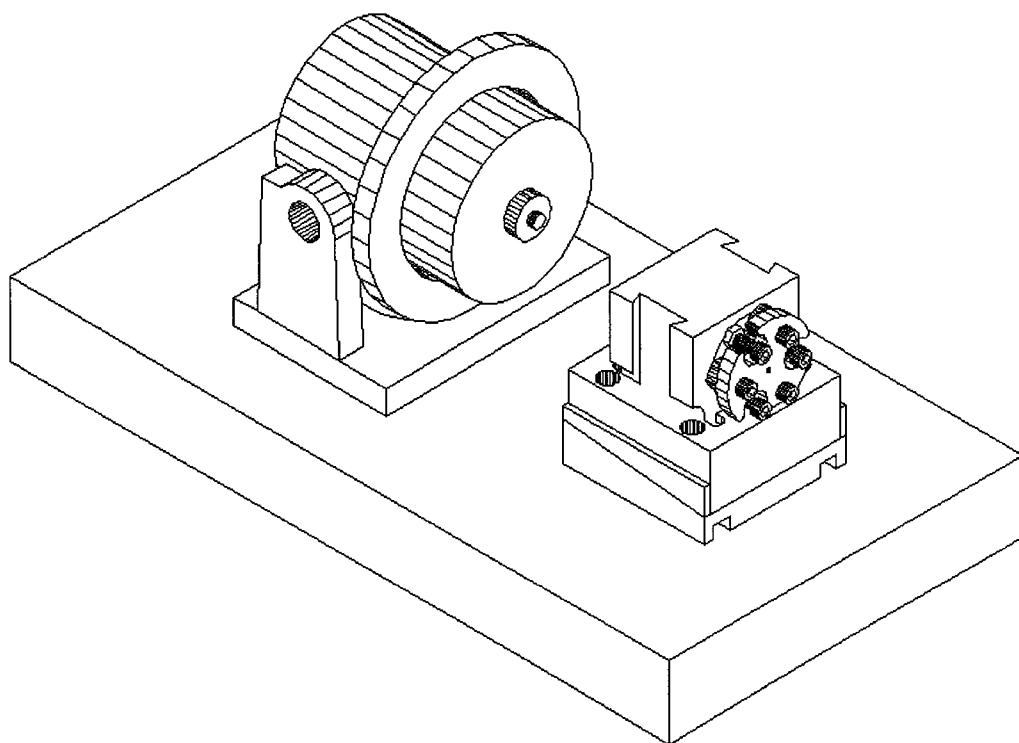
(a) Design aspect of the testbed
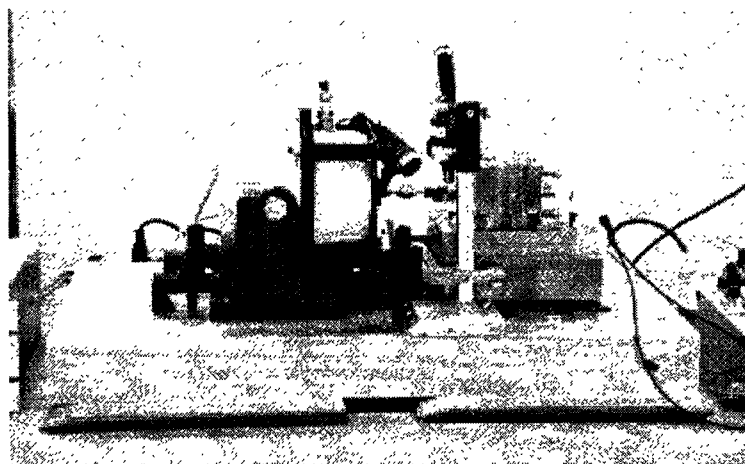


(b) A photo of the testbed

Figure 4-3  Experimental setup for testing the smart tool post structure

As shown in the figures above, the smart tool post structure sits on a special steel base platform. The platform is made up of two pieces. The inclined angle on each piece has been machined at 5.71° to yield a total of 3 mm travel distance for minor adjustment of the tool cutting tip to the center of the workpiece. The platform can be mounted on the Clausing Colchester 15" Lathe for stability as well as for increased stiffness during machining operation. Figure 4-4 shows the steel platform. Figure 4-5 shows how the steel platform is mounted onto the lathe.
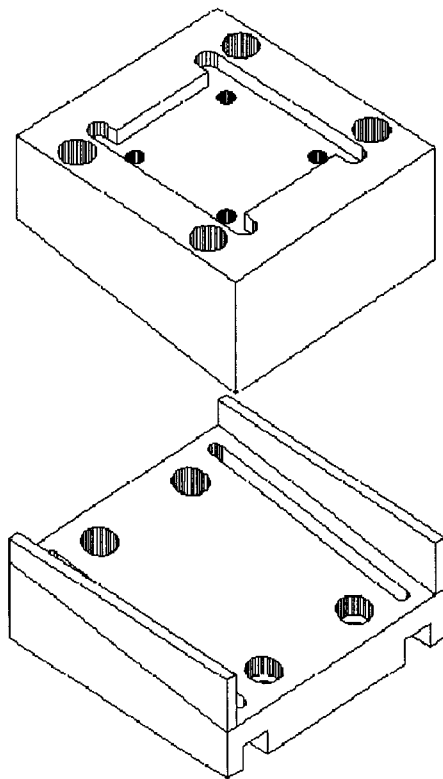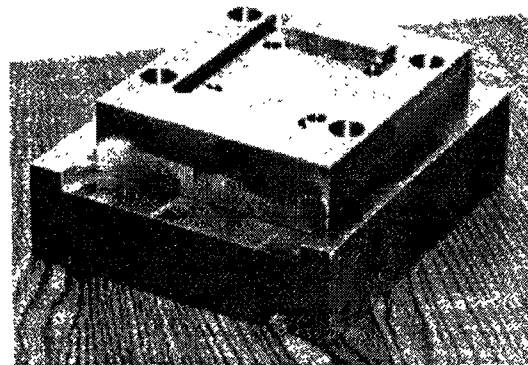


(a) Design concept                    (b) Final product

Figure 4-4  The base platform used to mount the smart tool post structure
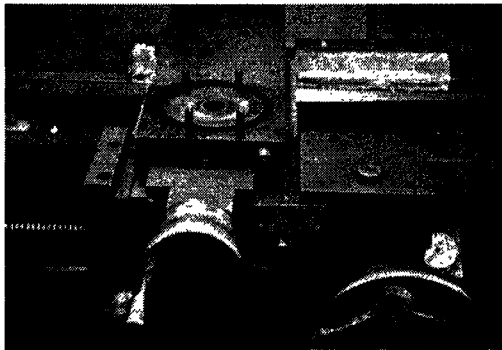
(a)  Original bolts on the Colchester Lathe
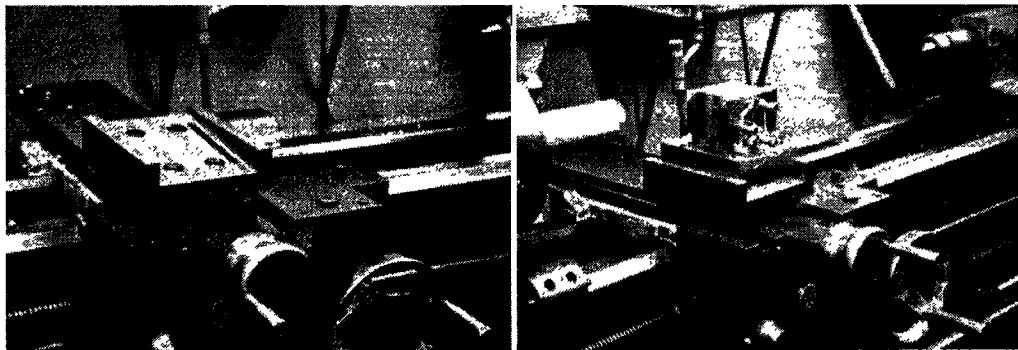


(b) The steel platform on the lathe     (c) Final assembly of the platform

Figure 4-5  Steel platform mounted onto the 15" Clausing Colchester Lathe



Adapter piece

Tool tip of the smart tool post
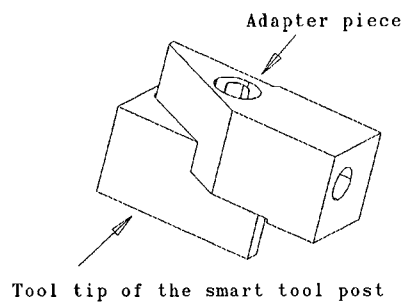
Figure 4-6  The adapter piece connecting the exciter to the tool post

Within the testbed, in order to monitor the force exerted by the exciter, a load cell is placed between the exciter and the tip of the smart tool post structure. As a result, an adapter piece is made to provide a connection between the two structures as shown in Figure 4-6. At the rear of the tool post, a non-contact displacement sensor is used to monitor the vibration signal. As a result, a special fixture has to be built to accommodate for the sensor. The mounting plate for the sensor is shown in the Figure 4-7. With the sensor fixture in place, the number of actuators that can be used for vibration compensation is limited to three.
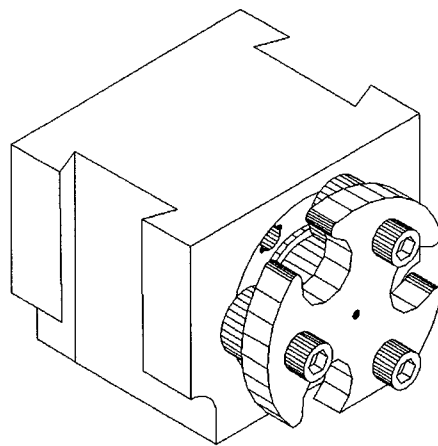


(a) Design concept for the mounting plate        (b) Product realization
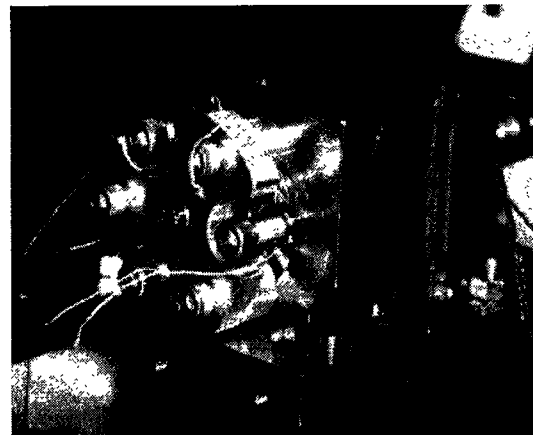
Figure 4-7 Mounting plate for the displacement sensor

In an actual machining operation, there is the presence of chips. To protect the VIT displacement sensor from flying chips as well as other foreign objects that may damage the sensor, a special housing structure was designed and built to encase the sensor inside the structure. The assembly of the sensor housing unit onto the

existing smart tool post structure is shown in Figure 4-8. A photo of the sensor

housing unit is shown in Figure 4-9.
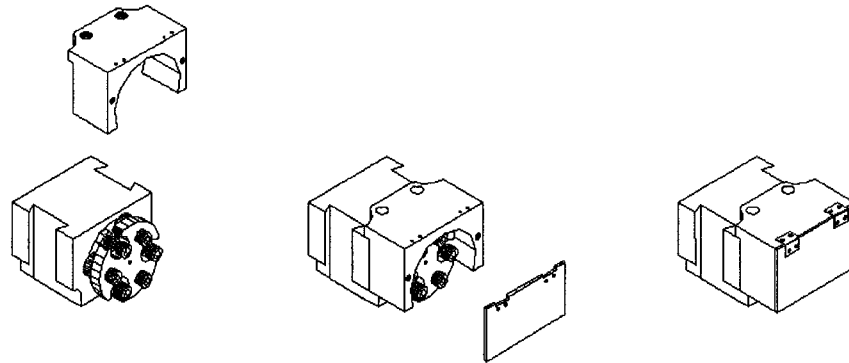


Figure 4-8 Assembly of the sensor housing unit onto the tool post structure
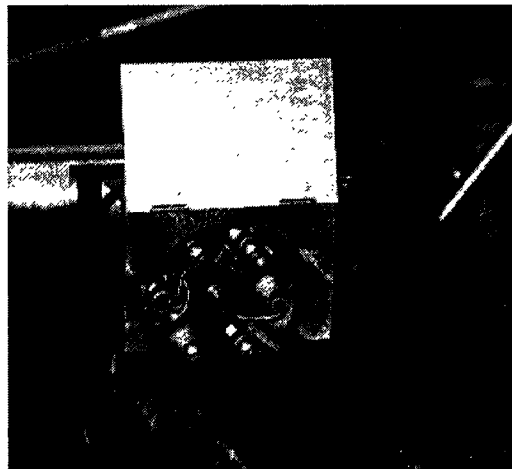


Figure 4-9 A photo of the sensor housing for the smart tool post

## 4.1.2 Application of Data Acquisition System

In order to control the collection and the analysis of data, a data acquisition

system from National Instruments Corporation was purchased and introduced into the experimentation environment. The data acquisition system consists of a 90 MHz computer, a 16-bit data acquisition board (DAQ board), a digital signal processing board (DSP board), and a signal conditioning unit with two signal conditioning modules. A summary of the data acquisition system is shown below. Details of hardware specifications and configurations are included in Appendix A.
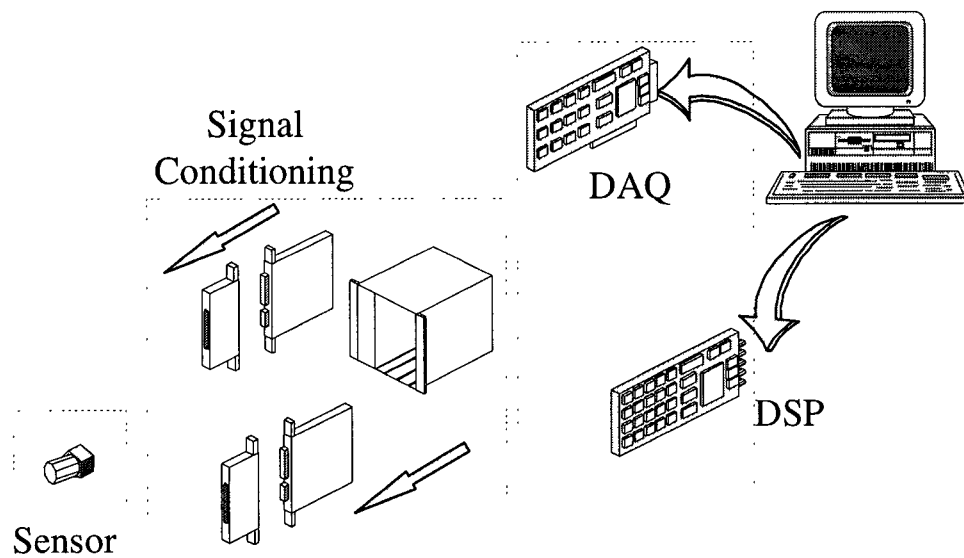


Figure 4-10 Components of the data acquisition system

As with any data acquisition system, the hardware of the system needs to be programmed by software. National Instruments, as one of the leading suppliers of data acquisition hardware and software for a variety of computer platforms and operating systems, has developed an innovative programming language called LabVIEW, a full development programming language to facilitate the programming task.

LabVIEW, which stands for <u>L</u>aboratory <u>V</u>irtual <u>I</u>nstrument <u>E</u>ngineering <u>W</u>orkbench, is a general-purpose program development application similar to other development systems such as C or BASIC. However, unlike these text-based development systems that create lines of codes, LabVIEW uses a graphical programming language simply called "G" to create block diagrams that compile into machine code. With its graphical capabilities, much of the work in syntactical details have been eliminated. As a result, LabVIEW can be used to solve many practical problems in a fraction of the time that it would take to write a conventional code. Since its development, some of the applications using LabVIEW are in simulating heart functions, controlling ice cream making process, and modeling power systems to analyze power quality.

With the data acquisition sets as shown above, physical data can be obtained from the transducers through the plug-in boards. Programs written in LabVIEW can be written to control everything from collecting the data to signal conditioning to analyzing the data to displaying the results for presentation. The graphical nature of LabVIEW makes the software ideal to capture the program's interface panel and paste it into a word processing application for documentation or presentation. Throughout this thesis work, programs written in LabVIEW are used to control the data acquisition system such as collecting machining data, analyzing the data collected, and simulating the machining environment by generating the excitation voltage to drive the exciter. The LabVIEW programs can be found in Appendix B.

## 4.2 Power Amplification to Drive the Actuators

Preliminary machining tests on the shop floor with the tool post structure revealed that the voltage to drive the actuators need to be increased from 10 Vrms to about 40 Vrms for vibration compensation. PMN actuators exhibit relatively high capacitance values, which are at about 6 $\mu$F. Specifications of the actuators can be found in Appendix C. Electrically, the actuators function as capacitors. Consequently, the impedance of the actuators is a function of the driving frequency. As the frequency of a power amplifier increases, the effective impedance of the actuators decreases, and so does the voltage drop on the actuators. Under circumstances where the impedance of a power amplifier to drive the actuators is comparable to the effective impedance of the actuators, driving the actuators becomes difficult because most of the power provided by the power amplifier is consumed by the power amplifier itself.

### 4.2.1 Wideband Power Amplifier System

In this research, the power amplifier used is the Krohn-Hite Amplifier Model 7602. Based on the specifications for output, an output of $\pm113$ V peak, 80V rms can be supplied for a 600 $\Omega$ load in a frequency range from 100 Hz to 1 M Hz. When the frequency range is between DC and 100 Hz, the output will be reduced to

±78 V dc and peak, 55V rms. For this reason, the circuit shown in Figure 4-11 was

designed in which a 100 Watts, 600 Ω resistor was used and it was connected in

series with a 6 μF actuator.

**600 Ω Resistor**
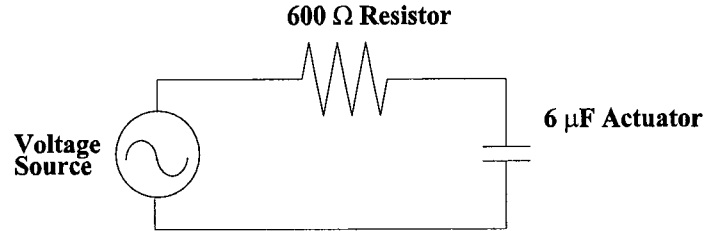


Figure 4-11  A schematic of the electrical circuit used to drive the actuator

The total impedance of the output under the driving frequency of 400 Hz is

given by

$$IMPENDANCE_{TOTAL} = \sqrt{R^2 + \left(\frac{1}{2\pi fc}\right)^2} \qquad (4\text{-}1)$$

$$= \sqrt{600^2 + \left(\frac{1}{2\pi(400)(6)(10^{-6})}\right)^2} = 600\ \Omega \quad (4\text{-}2)$$

In terms of power consumption, the capacitors and thus the actuators do not

dissipate but store energy.  The net energy transfer from the plant to the load is the

same as the average power.  As a result, the total power dissipated in the load is the

power dissipated in the load resistance.  Based on this concept, an experiment was

conducted at a frequency of 400 Hz and a multimeter was used to measure the

46

voltage across the resistor and the actuator. The voltage across the resistor was 40 V rms, and across the actuators was 15 V rms. Therefore, the impedance ratio of the resistor to the actuators matched the voltage drop ratio of the resistor to the actuator, which is approximately equal to 2.67. From the viewpoint of power consumption, the resistor consumed 2.75 watts and the actuator consumed 1.05 watts. Under this experimental condition, the efficiency of the power amplifier to drive the actuator was about 28 percent. This indicates that the amplifier was supplying 3.8 watts the entire circuit, with only 28 percent of the effective energy being supplied to the actuator. This low efficiency was due to an impedance mismatch.

### 4.2.2 Audio Power Amplifier System

To match the impedance between the power amplifier and the actuator, an audio amplifier and an audio transformer are introduced into the circuit. Since it was shown that 1.05 watts was being delivered to the actuators with the Krohn-Hite amplifier system. The energy delivered to the actuator was too low to allow the actuator to function appropriately. It is expected that a minimum of 5 watts would be needed. In the second stage of experimentation, a 60-watts audio amplifier was used to supply energy to the actuators. Specifications of the audio amplifier shows

that the amplifier can deliver an output of ±34 V peak, 24 V rms, for a 22 Ω load in

a frequency range from DC to 400 Hz.

The audio amplifier can deliver enough power, but its maximum output

voltage is only 24 V rms. Therefore, a step up transformer is necessary. A 5:1 step-

down audio transformer was used backward in the system as a 1:5 step-up

transformer. The transformer is a dual bobbin controller filament transformer, with

a 110 V primary and a 22 V secondary. The transformer is rated at 1 A at 22 V on

the secondary at 60 Hz, therefore its output impedance is approximately 22 Ω. The

primary impedance is approximately 110 Ω. The electrical circuit to enhance the

power requirement to drive the actuators is shown in Figure 4-12.
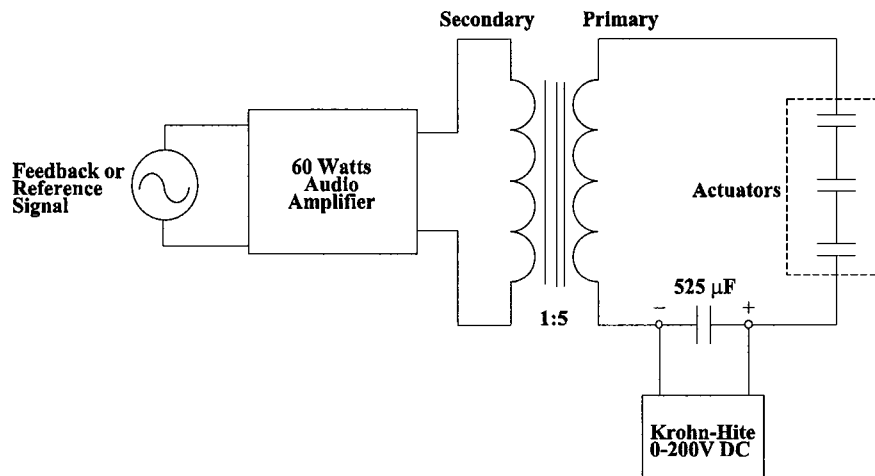
Figure 4-12 Circuit used to increase the voltage to drive the actuators

For proper operation, the actuators must be biased with a DC offset voltage.

However, using a transformer effectively AC-couples the system. As a result, a 525

µF capacitor and the Krohn-Hite amplifier were used to DC bias the actuators. The Krohn-Hite amplifier has its AC input shorted to ground, but the DC offset is used across the capacitor. The capacitor does add some impedance to the circuit, but it is below 2 Ω.

From the information given above, the impedance in the load can be approximated by Equation 4-3 and the average power can be calculated using Equation 4-5 [29].

$$I_L = \frac{V_s}{\sqrt{R^2 + \left(\dfrac{1}{j\omega C}\right)^2}} \qquad (4\text{-}3)$$

$$= \frac{120}{\sqrt{110^2 + \left(\dfrac{1}{j(2)(\pi)(400)(6)(10^{-6})}\right)^2}} = 0.9375 \qquad (4\text{-}4)$$

$$P_{AV} = \frac{I_L{}^2 R}{2} \qquad (4\text{-}5)$$

$$= \frac{(0.9375)^2(10)}{2} = 4.4\,Watts \qquad (4\text{-}6)$$

## 4.3   Experimentation within the Testbed Environment

Using the testbed and the data acquisition system setup described in the previous sections, experimental preparation and procedure were formulated to

49

evaluate the performance of the tool post system. A series of tests were conducted to define the roles played by the PMN actuators in the energy transformation from the electrical energy domain to the mechanical energy domain. To accomplish such a task, a previously designed phase-shift controller was employed. In particular, experiments were conducted with the tool post driven at single-frequency component and multiple-frequency component with the application of the phase-shift controller for vibration compensation. Results from such experiments are used to provide guidelines into implementing the tool post structure to a shop floor machining environment.

### 4.3.1 Experimental Preparation

Software as well as hardware preparation was required before actual experiments can be conducted. To generate excitation voltage to drive the exciter which in turn excites the tool post, a program was written in LabVIEW to generate sinusoidal signals at three different frequency components. The front panel of the wave generator is shown below. Within the program, the user can update the settings of any frequency component at any time. If only one frequency component is desired, the other two frequency components can be turned off by simply entering zeros to the corresponding amplitude and frequency input areas. The output of the generator was sent through one of the two output channels of the DSP board.

(Refer to Appendix B for the block diagram of the program.)
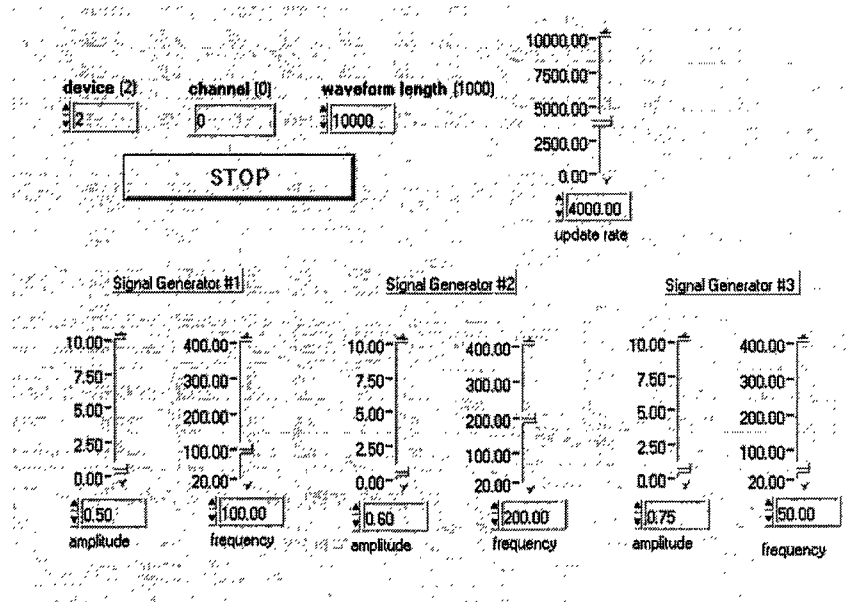


Figure 4-13 Front panel of the wave generator

A second LabVIEW program was written to monitor and collect the vibration signal due to the excitation from the exciter. The front panel of the program is shown below. In this program, the linear spectrum of the signal can be turned on or off. To interface this program with the controller circuitry, the phase-shift controller had to be modified to allow communication through a RS-232 cable. The RS-232 is a standard 9-pin cable. With such modifications, the program can send the frequency to the controller so that the proper time delay can be calculated based on the look-up table. The program has the flexibility to allow the user to the magnitude of the linear spectrum plot in a file for later analysis. In cases where the

users decide to add LabVIEW analytical tools such as for statistical calculations, these tools can be easily added.
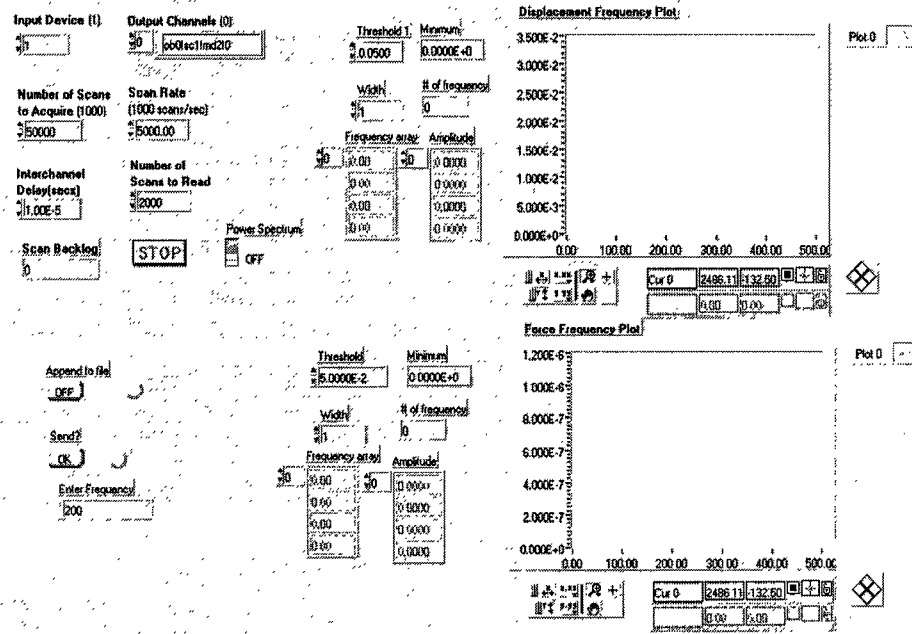


Figure 4-14  Program used to monitor the vibration during machining

## 4.3.2  Experimental Procedure and Results

To test the effectiveness of the phase-shift controller in reducing multiple driving frequencies, three experiments were conducted.   In the first two experiments, the tool post was driven at a single frequency to determine the relational effects of the controller in reducing the amplitude of excited vibration.  In the third experiment, the controller is tested by exciting the tool post using a signal with a summation of three frequency components.  The procedure and the results

for each of the three experiments are described below.

In the first experiment, the tool post is tested at a single driving frequency with three distinct driving vibration amplitude. The objective of this experiment is to determine the effect of the variation in the vibration amplitude when the tool post is driven at a single frequency between 100, 120, 140, ..., 400 Hz with and without the controller. The conditions of the tests are shown in Table 4-1 below.

Table 4-1  Test conditions for driving the tool post at one frequency

| Test No. | Frequency | A #1 | A #2 | A #3 |
|---|---|---|---|---|
| 1 | 100 | 0.50 | 0.75 | 1.00 |
| 2 | 120 | 0.50 | 0.75 | 1.00 |
| 3 | 140 | 0.50 | 0.75 | 1.00 |
| 4 | 160 | 0.50 | 0.75 | 1.00 |
| 5 | 180 | 0.50 | 0.75 | 1.00 |
| 6 | 200 | 0.50 | 0.75 | 1.00 |
| 7 | 220 | 0.50 | 0.75 | 1.00 |
| 8 | 240 | 0 50 | 0.75 | 1.00 |
| 9 | 260 | 0.50 | 0 75 | 1 00 |
| 10 | 280 | 0.50 | 0.75 | 1.00 |
| 11 | 300 | 0.50 | 0.75 | 1.00 |
| 12 | 320 | 0.50 | 0.75 | 1.00 |
| 13 | 340 | 0.50 | 0.75 | 1.00 |
| 14 | 360 | 0.50 | 0.75 | 1.00 |
| 15 | 380 | 0.50 | 0.75 | 1.00 |
| 16 | 400 | 0.50 | 0.75 | 1.00 |

At each driving frequency, the amplitude is changed from 0.50 to 0.75 to 1.00. At each change in the amplitude, the controller is turned on and off. The amplitude of the linear spectrum of the signal is recorded and the percent of reduction is calculated based on the spectrum amplitude. A plot summarizing the results is shown in Figure 4-15. As seen in the plot, there is no significance difference in the percent of reduction when the amplitude is changed at each driving frequency. However, at 380 and 400 Hz, there is evidence of increased in vibration

53

rather than attenuation. As a result, 380 Hz marks the upper functional limit of the controller.

In the second experiment, the tool post structure and the controller are also tested at a single driving frequency. However, the objective in this experiment is to determine the effect of the percent of reduction when different time delay in the controller is used. Table 4-2 below shows the test conditions used in the experiment. As stated in Dold's thesis [18], the time delay in the control loop is expressed as a function of frequency or

$$\text{Phase shift} = 191.252 - 0.613 * \text{frequency} \qquad (3\text{-}2)$$

As a result, the table below shows the frequency at which to send the time delays to the controller.

Table 4-2  Test conditions for testing different time delays in the controller

| Frequency | Amplitude | Frequency to compensate at | | | | | | | | | | | |
|---|---|---|---|---|---|---|---|---|---|---|---|---|---|
| 100 | 0.75 | 100 | 125 | 150 | 175 | 200 | 225 | 250 | 275 | 300 | 325 | 350 | 375 | 400 |
| 120 | 0.75 | 100 | 125 | 150 | 175 | 200 | 225 | 250 | 275 | 300 | 325 | 350 | 375 | 400 |
| 140 | 0.75 | 100 | 125 | 150 | 175 | 200 | 225 | 250 | 275 | 300 | 325 | 350 | 375 | 400 |
| 160 | 0.75 | 100 | 125 | 150 | 175 | 200 | 225 | 250 | 275 | 300 | 325 | 350 | 375 | 400 |
| 180 | 0.75 | 100 | 125 | 150 | 175 | 200 | 225 | 250 | 275 | 300 | 325 | 350 | 375 | 400 |
| 200 | 0.75 | 100 | 125 | 150 | 175 | 200 | 225 | 250 | 275 | 300 | 325 | 350 | 375 | 400 |
| 220 | 0.75 | 100 | 125 | 150 | 175 | 200 | 225 | 250 | 275 | 300 | 325 | 350 | 375 | 400 |
| 240 | 0.75 | 100 | 125 | 150 | 175 | 200 | 225 | 250 | 275 | 300 | 325 | 350 | 375 | 400 |
| 260 | 0.75 | 100 | 125 | 150 | 175 | 200 | 225 | 250 | 275 | 300 | 325 | 350 | 375 | 400 |
| 280 | 0.75 | 100 | 125 | 150 | 175 | 200 | 225 | 250 | 275 | 300 | 325 | 350 | 375 | 400 |
| 300 | 0.75 | 100 | 125 | 150 | 175 | 200 | 225 | 250 | 275 | 300 | 325 | 350 | 375 | 400 |
| 320 | 0.75 | 100 | 125 | 150 | 175 | 200 | 225 | 250 | 275 | 300 | 325 | 350 | 375 | 400 |
| 340 | 0.75 | 100 | 125 | 150 | 175 | 200 | 225 | 250 | 275 | 300 | 325 | 350 | 375 | 400 |
| 360 | 0.75 | 100 | 125 | 150 | 175 | 200 | 225 | 250 | 275 | 300 | 325 | 350 | 375 | 400 |
| 380 | 0.75 | 100 | 125 | 150 | 175 | 200 | 225 | 250 | 275 | 300 | 325 | 350 | 375 | 400 |
| 400 | 0.75 | 100 | 125 | 150 | 175 | 200 | 225 | 250 | 275 | 300 | 325 | 350 | 375 | 400 |
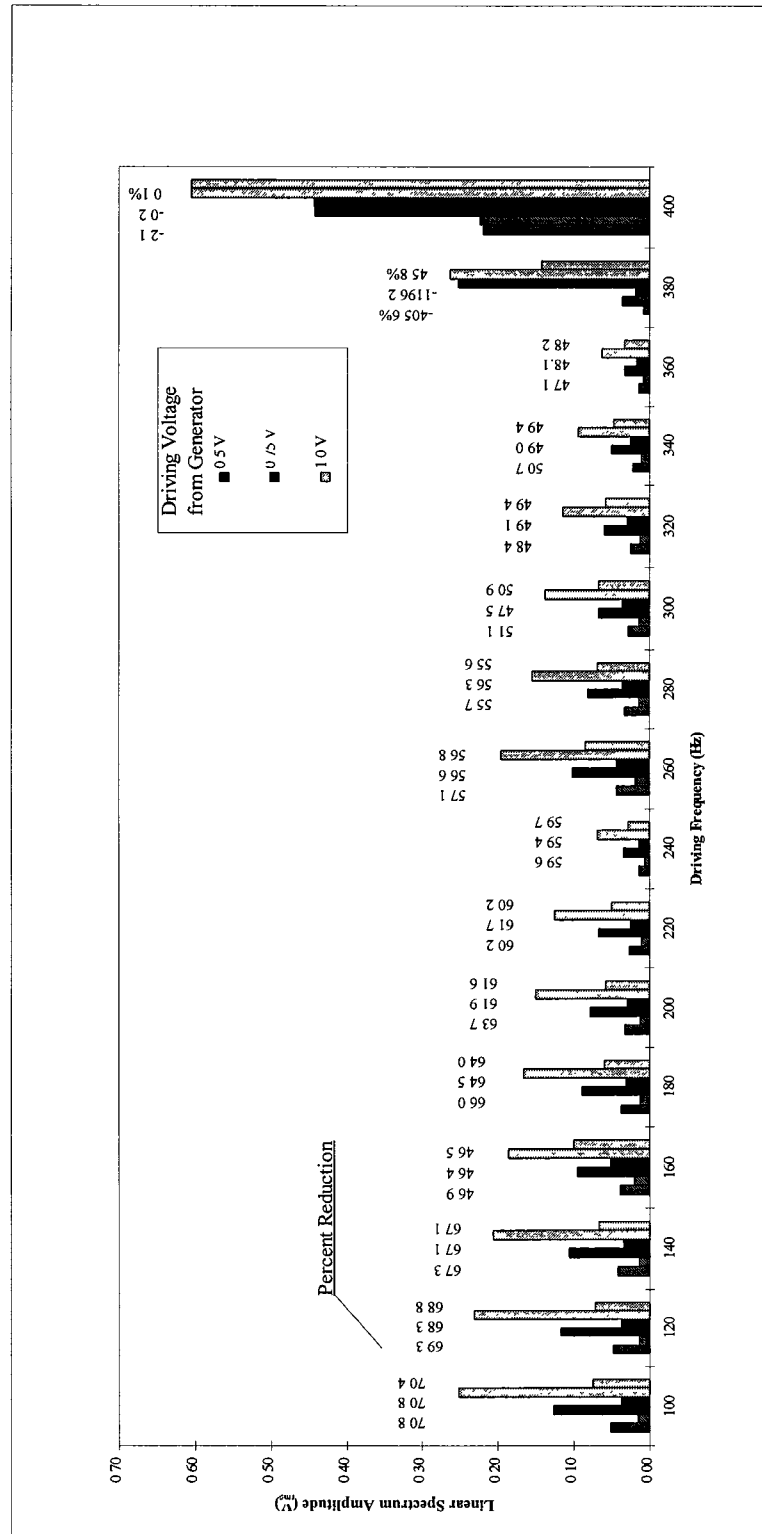
Figure 4-15  Results from using the controller at one frequency

55
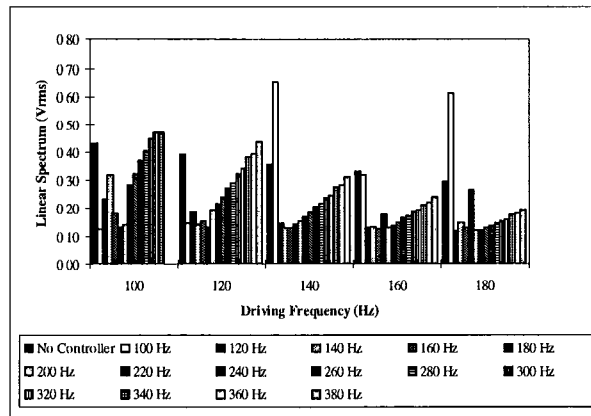
(a) 100 to 180 Hz driving frequency
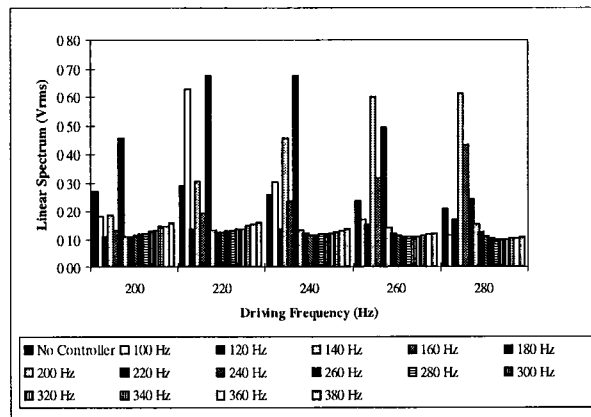


(b) 200 to 280 Hz driving frequency
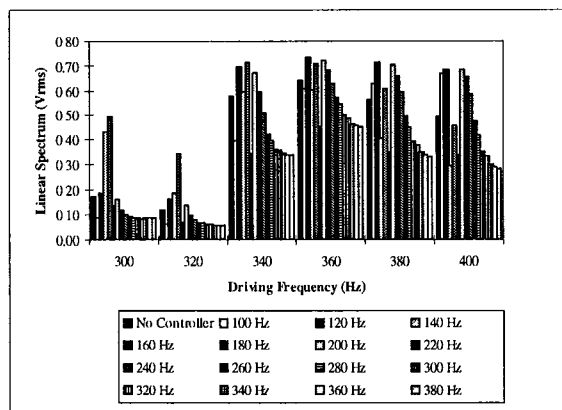


(c) 300 to 400 Hz driving frequency

Figure 4-16 Effects of compensation at different time delays

The results of the experiment are plotted in Figure 4-16. In general, the greatest reduction is seen when the time delay is set at the driving frequency. For instance, in Figure 4-16(a), the excitation frequency in the first set of data is at 100 Hz. By varying the frequency from no controller to 100 Hz to 380 Hz, it can be seen that the greatest reduction can be seen at 100 Hz. As the frequency in which to calculate the time delay gets further from the driving frequency, the vibration worsens. The extent of an increased in vibration can be seen in the plots.

The two experiments conducted above establish a procedure and an analytical method in which to deal with the vibration from the machining process where multiple frequencies components may be present. As a result, the third experiment conducted in the virtual machining environment attempts to evaluate the characteristics of the smart tool post structure when it is subjected to an excitation due to a summation of three different frequency components.

The third experiment was conducted based on a $2^6$ factorial design. The test conditions are shown below in Table 4-3. A typical plot of the result is shown in Figure 4-17. For each test condition, the linear spectrum of the time domain signal was plotted and the magnitude of the spectrum was recorded. Comparison was then made with the controller switched off and then switched on with the controller set at different phase shift value. Based on this design of experimentation, three conclusions can be made about the modified tool post structure.

First, in the presence of multiple frequency components in the vibration

signal, the frequency component with the greatest magnitude should be used to calculate the amount of phase shift in order to compensate for the signal. Observations had shown that by compensating the vibration at the frequency with the greatest magnitude can reduce up to 50 percent of the vibration over 75 percent of the time. At the other 25 percent of the time, little or no reduction can be seen. Second, depending on the ranges of the frequency components, phase shifting the vibration signal did not necessarily reduced the magnitude of other frequencies. Third, compensating at the wrong frequency resulted in creating instability in the system.

Table 4-3  Testing the tool post at three frequency component

|      | Gf#1 | Gf#2 | Gf#3 | Ga#1 | Ga#2 | Ga#3 |
|------|------|------|------|------|------|------|
| High | 140  | 270  | 400  | 0.75 | 1.1  | 1.5  |
| Low  | 20   | 150  | 280  | 0.5  | 0.85 | 1.25 |

| Test | Gf#1 | Gf#2 | Gf#3 | Ga#1 | Ga#2 | Ga#3 | Test | Gf#1 | Gf#2 | Gf#3 | Ga#1 | Ga#2 | Ga#3 |
|------|------|------|------|------|------|------|------|------|------|------|------|------|------|
| 1  | 140 | 270 | 400 | 0.75 | 1.10 | 1.50 | 33 | 140 | 270 | 400 | 0.75 | 1.10 | 1.25 |
| 2  | 20  | 270 | 400 | 0.75 | 1.10 | 1.50 | 34 | 20  | 270 | 400 | 0.75 | 1.10 | 1.25 |
| 3  | 140 | 150 | 400 | 0.75 | 1.10 | 1.50 | 35 | 140 | 150 | 400 | 0.75 | 1.10 | 1.25 |
| 4  | 20  | 150 | 400 | 0.75 | 1.10 | 1.50 | 36 | 20  | 150 | 400 | 0.75 | 1.10 | 1.25 |
| 5  | 140 | 270 | 280 | 0.75 | 1.10 | 1.50 | 37 | 140 | 270 | 280 | 0.75 | 1.10 | 1.25 |
| 6  | 20  | 270 | 280 | 0.75 | 1.10 | 1.50 | 38 | 20  | 270 | 280 | 0.75 | 1.10 | 1.25 |
| 7  | 140 | 150 | 280 | 0.75 | 1.10 | 1.50 | 39 | 140 | 150 | 280 | 0.75 | 1.10 | 1.25 |
| 8  | 20  | 150 | 280 | 0.75 | 1.10 | 1.50 | 40 | 20  | 150 | 280 | 0.75 | 1.10 | 1.25 |
| 9  | 140 | 270 | 400 | 0.50 | 1.10 | 1.50 | 41 | 140 | 270 | 400 | 0.50 | 1.10 | 1.25 |
| 10 | 20  | 270 | 400 | 0.50 | 1.10 | 1.50 | 42 | 20  | 270 | 400 | 0.50 | 1.10 | 1.25 |
| 11 | 140 | 150 | 400 | 0.50 | 1.10 | 1.50 | 43 | 140 | 150 | 400 | 0.50 | 1.10 | 1.25 |
| 12 | 20  | 150 | 400 | 0.50 | 1.10 | 1.50 | 44 | 20  | 150 | 400 | 0.50 | 1.10 | 1.25 |
| 13 | 140 | 270 | 280 | 0.50 | 1.10 | 1.50 | 45 | 140 | 270 | 280 | 0.50 | 1.10 | 1.25 |
| 14 | 20  | 270 | 280 | 0.50 | 1.10 | 1.50 | 46 | 20  | 270 | 280 | 0.50 | 1.10 | 1.25 |
| 15 | 140 | 150 | 280 | 0.50 | 1.10 | 1.50 | 47 | 140 | 150 | 280 | 0.50 | 1.10 | 1.25 |
| 16 | 20  | 150 | 280 | 0.50 | 1.10 | 1.50 | 48 | 20  | 150 | 280 | 0.50 | 1.10 | 1.25 |
| 17 | 140 | 270 | 400 | 0.75 | 0.85 | 1.50 | 49 | 140 | 270 | 400 | 0.75 | 0.85 | 1.25 |
| 18 | 20  | 270 | 400 | 0.75 | 0.85 | 1.50 | 50 | 20  | 270 | 400 | 0.75 | 0.85 | 1.25 |
| 19 | 140 | 150 | 400 | 0.75 | 0.85 | 1.50 | 51 | 140 | 150 | 400 | 0.75 | 0.85 | 1.25 |
| 20 | 20  | 150 | 400 | 0.75 | 0.85 | 1.50 | 52 | 20  | 150 | 400 | 0.75 | 0.85 | 1.25 |
| 21 | 140 | 270 | 280 | 0.75 | 0.85 | 1.50 | 53 | 140 | 270 | 280 | 0.75 | 0.85 | 1.25 |
| 22 | 20  | 270 | 280 | 0.75 | 0.85 | 1.50 | 54 | 20  | 270 | 280 | 0.75 | 0.85 | 1.25 |
| 23 | 140 | 150 | 280 | 0.75 | 0.85 | 1.50 | 55 | 140 | 150 | 280 | 0.75 | 0.85 | 1.25 |
| 24 | 20  | 150 | 280 | 0.75 | 0.85 | 1.50 | 56 | 20  | 150 | 280 | 0.75 | 0.85 | 1.25 |
| 25 | 140 | 270 | 400 | 0.50 | 0.85 | 1.50 | 57 | 140 | 270 | 400 | 0.50 | 0.85 | 1.25 |
| 26 | 20  | 270 | 400 | 0.50 | 0.85 | 1.50 | 58 | 20  | 270 | 400 | 0.50 | 0.85 | 1.25 |
| 27 | 140 | 150 | 400 | 0.50 | 0.85 | 1.50 | 59 | 140 | 150 | 400 | 0.50 | 0.85 | 1.25 |
| 28 | 20  | 150 | 400 | 0.50 | 0.85 | 1.50 | 60 | 20  | 150 | 400 | 0.50 | 0.85 | 1.25 |
| 29 | 140 | 270 | 280 | 0.50 | 0.85 | 1.50 | 61 | 140 | 270 | 280 | 0.50 | 0.85 | 1.25 |
| 30 | 20  | 270 | 280 | 0.50 | 0.85 | 1.50 | 62 | 20  | 270 | 280 | 0.50 | 0.85 | 1.25 |
| 31 | 140 | 150 | 280 | 0.50 | 0.85 | 1.50 | 63 | 140 | 150 | 280 | 0.50 | 0.85 | 1.25 |
| 32 | 20  | 150 | 280 | 0.50 | 0.85 | 1.50 | 64 | 20  | 150 | 280 | 0.50 | 0.85 | 1.25 |
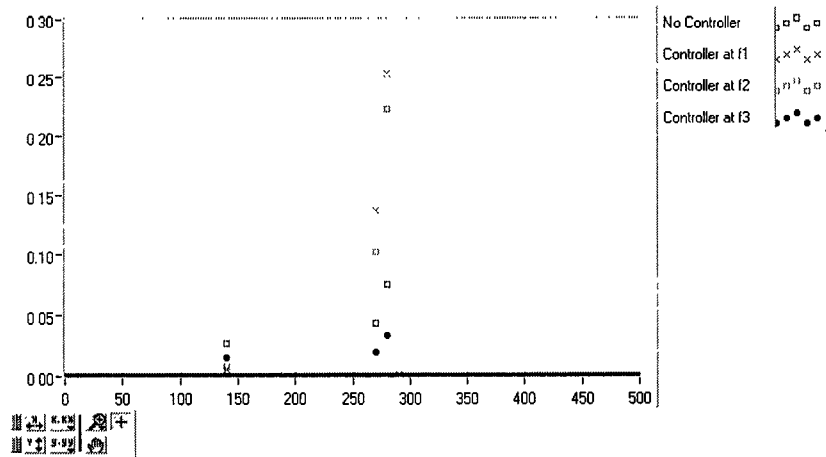
Figure 4-17  LabVIEW linear spectrum plot of the result

# Chapter 5

# Shop Floor Machining Environment

## 5.1 Strategies for Shop Floor Experimentation

Although the transition between the experimental testbed environment and the shop floor environment was minor, several specific preparations were required before actual experimentation could be conducted on the shop floor. In particular, the data acquisition program to be used in the shop floor environment was expanded and became more sophisticated in order to accommodate for a faster sampling rate. In addition, a series of preliminary machining tests was necessary in order to test and determine the gain setting, the filtering envelope, and the appropriateness of the sensor's range and resolution.

### 5.1.1 Data Acquisition

Using the data acquisition system as described in Chapter 4, a LabVIEW program is specifically written to collect the vibration signal during machining and write or stream the data to file while the data collection is in progress. To keep up

with the data acquisition rate and prevent data overflow in the memory buffer, the program incorporates features that can be switched on and off. The features of the program include the following: turning on the linear spectrum function to compute the FFT of the signal, turning on a bandpass Butterworth filter, streaming data to disk in binary format while continuously collect the data, communicating with the phase-shift controller through the RS-232 cable, reading data back from the disk, and converting the data from binary format into ASCII format. By writing in binary format during the collection of data, the ASCII-text conversion process is avoided resulting in using less computational time and saving storage file size.

The program described above is named lathe.llb. Lathe.llb is a LabVIEW library file made up of four other LabVIEW subprograms or subVIs. At each call to a subVI, the front panel of that subVI will appear thus allowing only the functions specific to that subVI to be executed. The flowchart and the front panel of the program are shown in Figure 5-1 and Figure 5-2, respectively. As can be seen in the front panel of the program, the user has four choices of buttons to select: scope, stream data to file, view data from file, and exit program. A click of the mouse at any of these button will execute the corresponding subVI. Figure 5-3, 5-4, and 5-5 show the front panel of the scope, the stream-data-to-file, the view-data-from file, respectively. For data analysis, the binary-formatted data file can be read and converted to ASCII-text format. The data then can be analyzed by using programs written in LabVIEW or other commercially available computational tools such as

MatLab. In this thesis work, various analytical tools were used for data analysis.
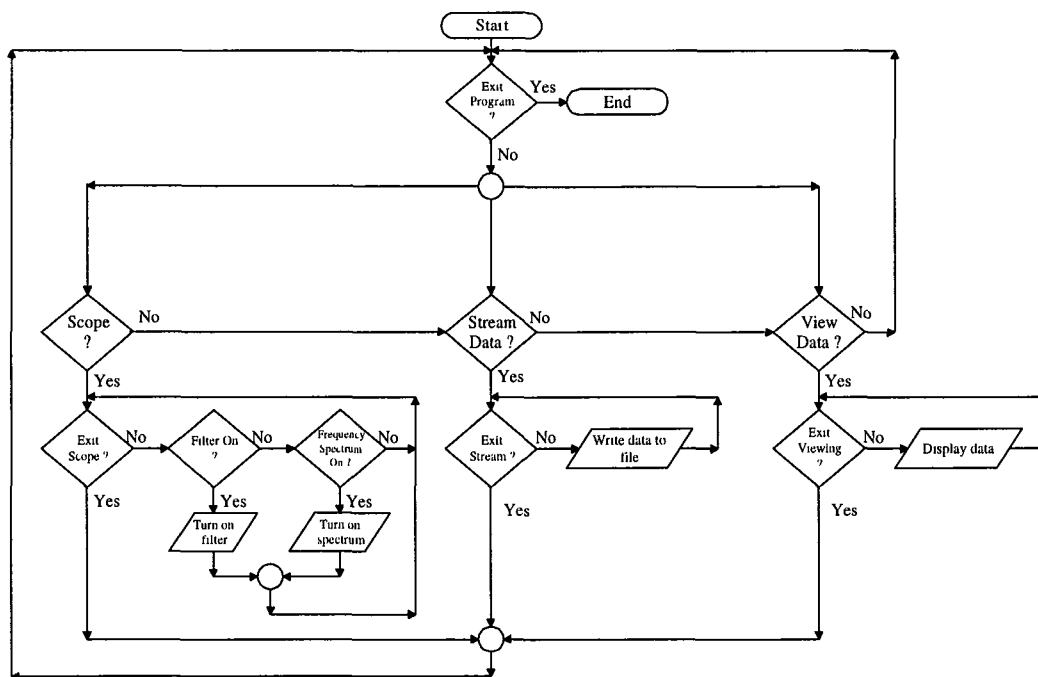


Figure 5-1  A flowchart showing the program logic
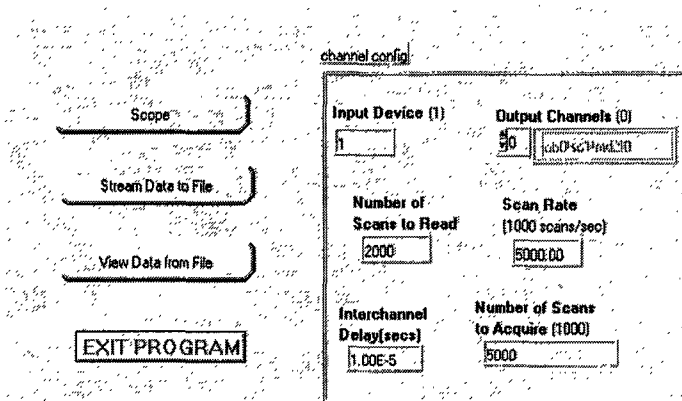


Figure 5-2  The front panel of the lathe.llb program
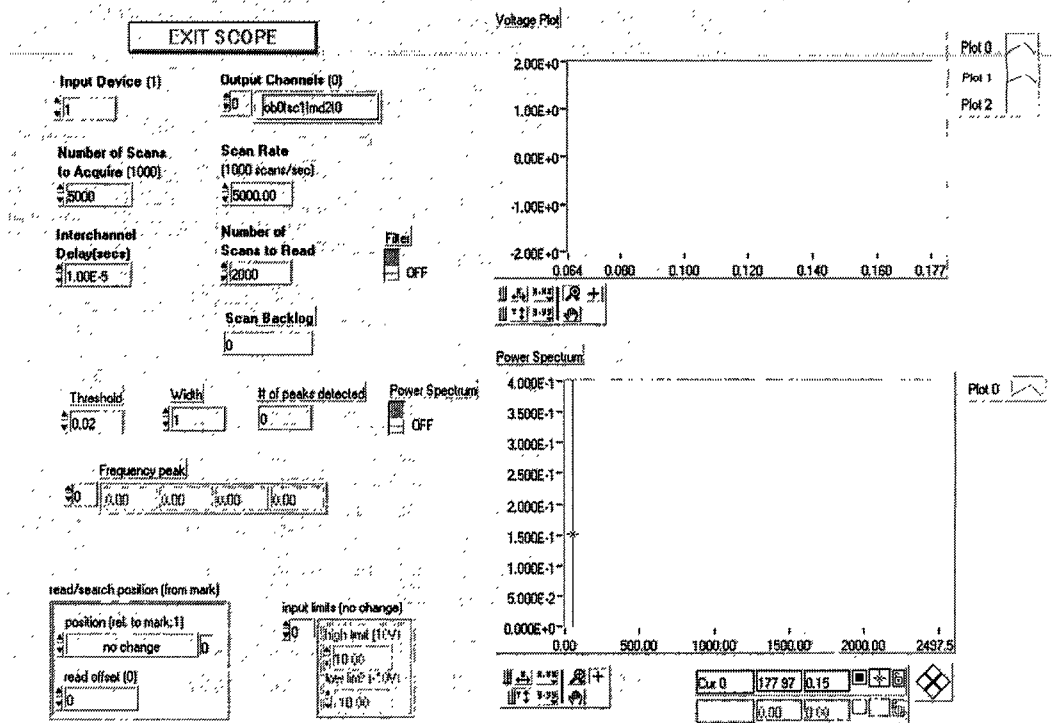
Figure 5-3  The front panel of the scope subVI program
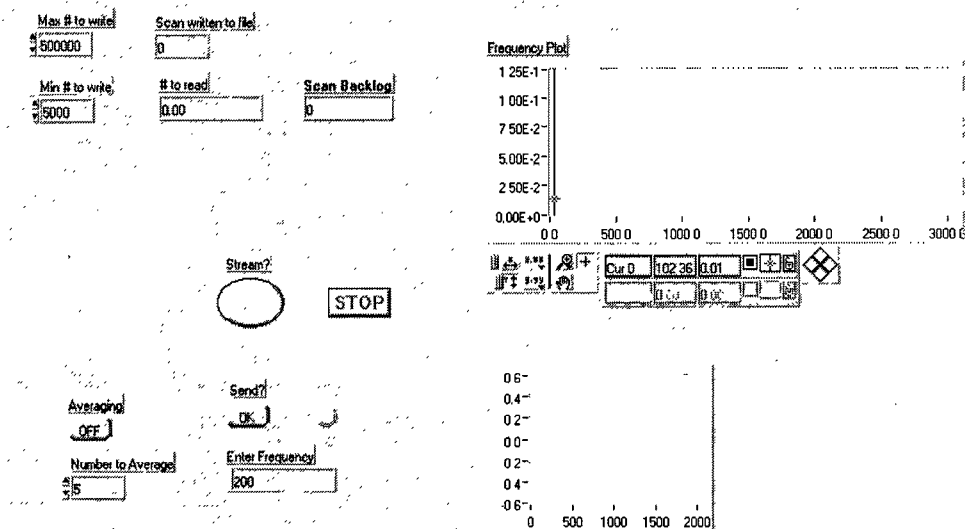


Figure 5-4  The front panel of the stream-data-to-file subVI program
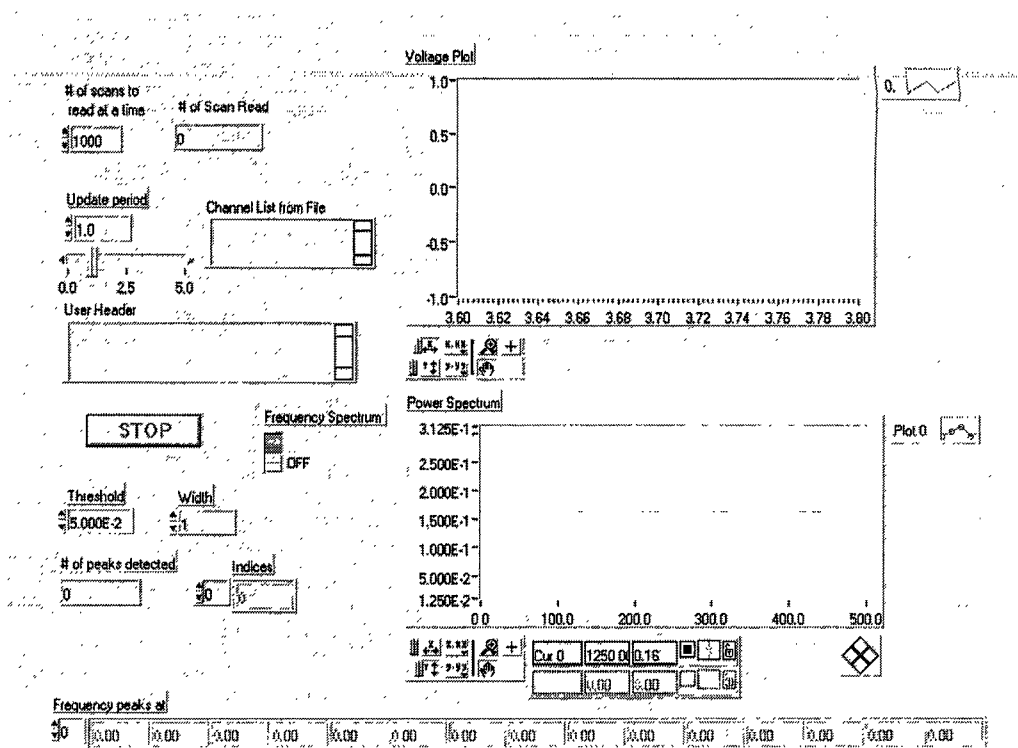
Figure 5-5  The front panel of the view-data-from-file subVI program

## 5.1.2  Experimental Procedure

Four sets of experiments were conducted on the shop.  In experimental set one, the objective was to determine the effects of the actuators on the machining vibration.  Machining tests were conducted using the tool post without and with the actuators installed.  For tests with the actuators installed, no power was supplied to the actuators.  In the second set of experiments, the power amplification was tested to determine whether or not the actuating force from the actuators alone can make dents on the surface.  In this set of experiments, up to 40 V rms was supplied to

each of the actuators. If the actuators cannot make a difference on the surface quality by their actuating force, then it is impossible for any type of vibration compensation to occur when the controller is applied. In experimental set three, power is supplied to the actuators to observe the roles of the actuators in attenuating the machining vibration. The frequency and the voltage settings of the power supply were manually adjusted for the best settings. In the fourth and final set of experiment, the previously designed phase-shift controller was tested to evaluate its performance and functionality. A summary of the experiments to be performed can be found in Table 5-1.

Table 5-1 Sets of experiments performed on the tool post

| Experimental Set | Descriptions |
|------------------|--------------|
| One | Test without and with actuators installed (but no power supplied) |
| Two | Drive the actuators to dent the surface |
| Three | Test power supply frequency and voltage for vibration compensation |
| Four | Test phase-shift controller for vibration compensation |

The workpiece material used during all four sets of experiments was Aluminum 6061-T16 rods with 3 in (76 mm) in diameter and 12 in (305 mm) in length. Six rods was used in the experiments. For identification purposes, the rods were identified as Rod1 to Rod6. Of the four sets of experiments, only the workpiece used in experimental set three for testing the power supply frequency and voltage were specially prepared into slots as shown in Figure 5-6. During all four sets of experiments, vibration signal from the VIT sensors was recorded. The

machining surface was preserved for Experimental Set Two, Three, and Four in order to obtain surface profile traces using a profilometer.
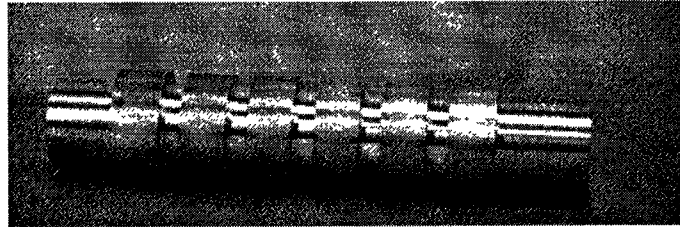


Figure 5-6 Slotted aluminum workpiece

## 5.2 Experimental Results and Discussion

The following sections present the results and the discussion of the four sets of experiments conducted on the shop floor based on the procedure described in the previous section.

### 5.2.1 Experimental Set One: Without and With Actuators

The two aluminum workpieces used in this set of experiments were named Rod1 and Rod2. The machining conditions used to machine Rod1 and Rod2 is shown in Table 5-2. Rod1 was machined without actuators and Rod2 was machined with three actuators prestressed. Table 5-3 summarizes the magnitude of displacement for both Rod1 and Rod2. Figure 5-7 shows the displacement plots for

Rod1 and Rod2 machined at 190 RPM, 0.02 in (0.50 mm) depth of cut, and 0.02 in/rev (0.50 mm/rev). The first four to five seconds of the displacement plots represent data collected without cutting. As a result, this portion of the data represents the background noise level of the vibration signal.

Table 5-2 Cutting parameters and test conditions used for machining tests

|  | Var. 1 D.O.C. (in) | Var. 2 Feed Rate (in/rev) | Var. 3 Spindle Speed (rpm) |
|---|---|---|---|
| Low | 0.020 (0.50 mm) | 0.002 (0.05 mm/rev) | 190 |
| High | 0.040 (1.02 mm) | 0.02 (0.50 mm/rev) | 470 |

$2^3$ FACTORIAL DESIGN

| Test Condition | D.O.C. (in) | Feed Rate (in/rev) | Spindle Speed (rpm) |
|---|---|---|---|
| 1 | 0.020 (0.50 mm) | 0.002 (0.05 mm/rev) | 190 |
| 2 | 0.040 (1.02 mm) | 0.002 (0.05 mm/rev) | 190 |
| 3 | 0.020 (0.50 mm) | 0.02 (0.50 mm/rev) | 190 |
| 4 | 0.040 (1.02 mm) | 0.02 (0.50 mm/rev) | 190 |
| 5 | 0.020 (0.50 mm) | 0.002 (0.05 mm/rev) | 470 |
| 6 | 0.040 (1.02 mm) | 0.002 (0.05 mm/rev) | 470 |
| 7 | 0.020 (0.50 mm) | 0.02 (0.50 mm/rev) | 470 |
| 8 | 0.040 (1.02 mm) | 0.02 (0.50 mm/rev) | 470 |

Table 5-3 Displacement magnitude of vibration

| Spindle Speed (rpm) | Feed Rate (in/rev) | Depth of Cut (in) | rod2 Vibration Magnitude ($\mu$in) | rod1 Vibration Magnitude ($\mu$in) | Percent Reduction (%) |
|---|---|---|---|---|---|
| 470 | 0.020 (0.50 mm/rev) | 0.02 (0.50 mm) | 9.8 (0.25 $\mu$m) | 49.2 (1.25 $\mu$m) | 80 |
| 470 | 0.020 (0.50 mm/rev) | 0.04 (1.02 mm) | 19.7 (0.50 $\mu$m) | 49.2 (1.25 $\mu$m) | 60 |
| 190 | 0.020 (0.50 mm/rev) | 0.02 (0.50 mm) | 15.7 (0.40 $\mu$m) | 49.2 (1.25 $\mu$m) | 68 |
| 190 | 0.020 (0.50 mm/rev) | 0.04 (1.02 mm) | 31.8 (0.80 $\mu$m) | 98.4 (2.50 $\mu$m) | 68 |
| 470 | 0.002 (0.05 mm/rev) | 0.02 (0.50 mm) | 2.0 (0.05 $\mu$m) | 7.9 (0.20 $\mu$m) | 75 |
| 470 | 0.002 (0.05 mm/rev) | 0.04 (1.02 mm) | 2.0 (0.05 $\mu$m) | 5.9 (0.15 $\mu$m) | 67 |
| 190 | 0.002 (0.05 mm/rev) | 0.02 (0.50 mm) | 1.2 (0.03 $\mu$m) | 7.9 (0.20 $\mu$m) | 88 |
| 190 | 0.002 (0.05 mm/rev) | 0.04 (1.02 mm) | 2.0 (0.05 $\mu$m) | 7.9 (0.20 $\mu$m) | 75 |
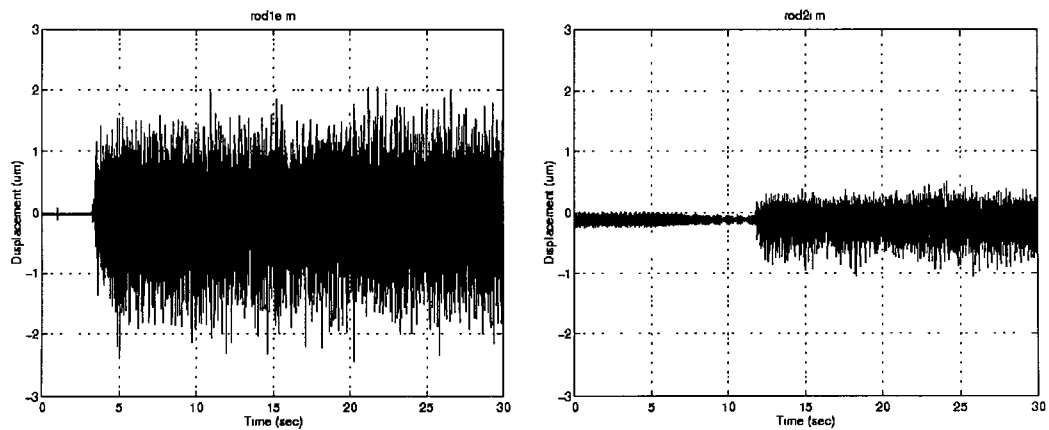
(a) Rod1     (b) Rod2

Figure 5-7 Displacement plots for Rod1 and Rod2

By machining the two aluminum rods, several important findings were observed about the performance of the tool post structure without and with the actuators installed.

1. The VIT sensor offers on average a 5:1 signal-to-noise ratio during machining. In general, the noise level is less than 1 μin (0.025 μm) as given in the specifications. As a result, the selection of the VIT sensor to be used in the machining environment is quite appropriate.

2. As shown in Table 5-2 above, installing the actuators create a drastic increase in the stiffness of the actuators. As a result, by installing three actuators, the magnitude of vibration reduced on average by about 70 percent.

## 5.2.2 Experimental Set Two: Actuating Force from Actuators

To test the effectiveness of the power amplification system to drive the actuators, ten slots on Rod3 was machined. The machining conditions for all ten slots were the same which was at 0.01 in (0.25 mm) depth of cut with a feed rate of 0.002 in/rev (0.05 mm/rev). The changing variable was the spindle speed. The spindle speed used is listed in Table 5-4. Five of the ten slots was machined without supplying power to the actuators to be used as referenced surfaces. The remaining five slots were machined with power supply to the actuators. For the slots machined with power supplied to the actuators, the DC bias offset was set at 164 V DC and the AC voltage was approximately 40 V rms at 300 Hz. During the machining, the data acquisition was not used to record the data since the magnitude of the vibration was out of range of the data acquisition card.

Table 5-4  The spindle speed used to test the power amplification system

| Slot | Surface Photos | Spindle Speed (RPM) |
|------|----------------|---------------------|
| 1 & 2 | (a) | 350 |
| 3 & 4 | (b) | 190 |
| 5 & 6 | (c) | 108 |
| 7 & 8 | (d) | 60 |
| 9 & 10 | (e) | 33 |

40 μin (1.01 μm)          23 μin (0.58 μm)          38 μin (0.96 μm)          18 μin (0.46 μm)



(a) 350 RPM                                        (b) 190 RPM

41 μin (1.04 μm)          19 μin (0.48 μm)          66 μin (1.68 μm)          17 μin (0.44 μm)



(c) 108 RPM                                        (d) 60 RPM

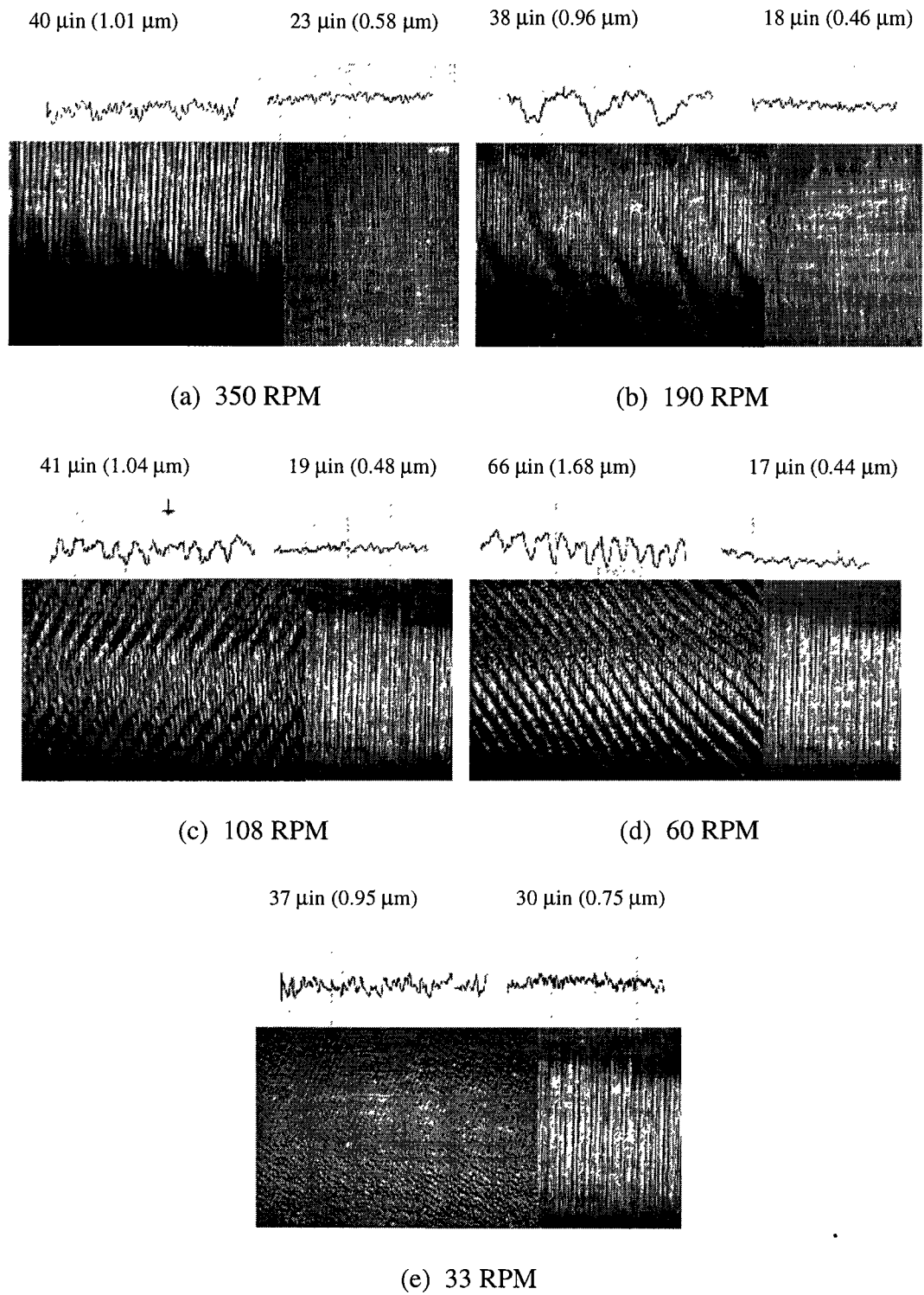37 μin (0.95 μm)          30 μin (0.75 μm)



(e) 33 RPM

Figure 5-8  Effects of driving the actuators using the power amplification

70

Figure 5-8 (a) - (e) show the machined surfaces without and with power supplied to the actuators starting from right to left on each of the photos. Additionally, the surface profile and the Ra value measurement for each of the surfaces are also included. As seen in the figure, the machined surfaces with power applied to the actuators were rougher. Therefore, it can be concluded that the power amplification is working as expected and that the actuators have the capability to provide the opposing force to compensate for the vibration during machining. Based on the surface profiles, the Ra measurement value, and the photos of the machine surface, the following observations can be made:

1.  The power supply system is very effective in driving the actuators. In fact, the actuators can be driven hard enough to make visible marks on the surface of the aluminum workpiece. As a result, the actuators have the force and the energy for vibration compensation. Success in achieving vibration compensation during machining depends on the success of controlling the actuating force.

2.  The type of marks and the surface quality of the workpiece change as the spindle speed changes. It can be seen that the surface quality at 33 rpm is comparable to the reference surface. Therefore, it is expected that the frequency as well as the magnitude of the driving force will be a factor in attentuating the vibration during machining.

71

### 5.2.3  Experimental Set Three:  Frequency and Gain Selection

Before machining experiments were conducted, characterization of the power amplifier was conducted to study the effect of frequency and the gain in driving the actuators. The result of the characterization is shown in Table 5-5.

Table 5-5  Power amplifier characterization

| Frequency (Hz) | Voltage from Amplifier (V rms) | | | |
|---|---|---|---|---|
| | Set 1 | Set 2 | Set 3 | Set 4 |
| 60 | 13.8 | 9.9 | 6.8 | 1.7 |
| 100 | 12.9 | 9.2 | 6.3 | 1.5 |
| 150 | 11.5 | 8.2 | 5.7 | 1.4 |
| 210 | 10.2 | 7.3 | 5.0 | 1.2 |
| 240 | 9.9 | 7.0 | 4.8 | 1.2 |
| 300 | 9.8 | 5.9 | -- | -- |
| 600 | 5.9 | 4.4 | -- | -- |
| 900 | 1.4 | 0.7 | -- | -- |

Table 5-6  Machining conditions used in conducting experimental set three

| | Var. 1 D.O.C. (in) | Var. 3 Spindle Speed (rpm) |
|---|---|---|
| Low | 0.040 (1.02 mm) | 470 |
| High | 0.060 (1.52 mm) | 625 |

$2^2$ FACTORIAL DESIGN

| Test Condition | D.O.C. (in) | Spindle Speed (rpm) |
|---|---|---|
| 1 | 0.040 (1.02 mm) | 470 |
| 2 | 0.060 (1.52 mm) | 470 |
| 3 | 0.040 (1.02 mm) | 625 |
| 4 | 0.060 (1.52 mm) | 625 |

Based on the information provided about the amplifier characteristics, the machining tests were then conducted. For this set of experiments, the machining conditions selected to determine the optimal frequency and gain settings to drive the actuators for vibration compensation are listed in Table 5-6 with the feed rate kept constant at 0.003 in/rev (0.08 mm/rev), the initial voltage to drive the actuators at 25 V rms, and the initial frequency at 900 Hz.

Using the machining conditions in Table 5-6 as a reference starting point, the spindle speed, the frequency to drive the actuators, and the voltage supplied to the actuators were shifted up and down to identify the optimal region for vibration compensation. Table 5-7 shows the frequency and voltage settings used in the machining tests. Machining started with no power supplied to the actuators. After the first 0.5 in (12.7 mm), the power supply was switched on with the gain slowly increased. Throughout the tests, an oscilloscope was used to monitor the vibration signal. As soon as any large fluctuation was observed in the displacement, the gain setting was lowered.

Consideration was taken in driving the actuators to avoid exciting the tool post at its natural frequencies. The natural frequencies of the tool post structure are listed in Table 5-8. The natural frequencies were obtained from impulse hammer tests as well as had been verified by exciting the tool post structure through a sinusoidal frequency sweeps.

Table 5-7  Settings used for selecting the proper frequency and gain

| Section ID | D.O.C. (in) | Feed Rate (in/rev) | Spindle Speed (rpm) | Driving Frequency (Hz) | Driving Voltage (Vrms) |
|---|---|---|---|---|---|
| Slot 4_1 | 0.040 (1.02 mm) | 0.003 (0.08 mm/rev) | 625 | 900 | 25 |
| Slot 4_2 | 0.040 (1.02 mm) | 0.003 (0.08 mm/rev) | 470 | 900 | 25 |
| Slot 4_3 | 0.040 (1.02 mm) | 0.003 (0.08 mm/rev) | 350 | 900 | 25 |
| Slot 4_4 | 0.040 (1.02 mm) | 0.003 (0.08 mm/rev) | 625 | 900 | 25 to 40 |
| Slot 4_5 | 0.040 (1.02 mm) | 0.003 (0.08 mm/rev) | 625 | 900 to 1200 | 15 to 25 |
| Slot 4_6 | 0.040 (1.02 mm) | 0.003 (0.08 mm/rev) | 625 | 900 to 1200 | 15 to 25 |

(a)  Parameters used for Rod4

| Section ID | D.O.C. (in) | Feed Rate (in/rev) | Spindle Speed (rpm) | Driving Frequency (Hz) | Driving Voltage (Vrms) |
|---|---|---|---|---|---|
| Slot 5_1 | 0.060 (1.52 mm) | 0.003 (0.08 mm/rev) | 625 | 900 | 25 |
| Slot 5_2 | 0.060 (1.52 mm) | 0.003 (0.08 mm/rev) | 470 | 900 | 25 |
| Slot 5_3 | 0.060 (1.52 mm) | 0.003 (0.08 mm/rev) | 350 | 900 | 25 |
| Slot 5_4 | 0.060 (1.52 mm) | 0.003 (0.08 mm/rev) | 625 | 900 | 25 to 40 |
| Slot 5_5 | 0.060 (1.52 mm) | 0.003 (0.08 mm/rev) | 625 | 900 to 1200 | 15 to 25 |
| Slot 5_6 | 0.060 (1.52 mm) | 0.003 (0.08 mm/rev) | 625 | 900 to 1200 | 15 to 25 |

(b)  Parameters used for Rod5

Table 5-8  Natural frequencies of the tool post structure

| | 1st Mode (Hz) | 2nd Mode (Hz) |
|---|---|---|
| Without Actuators | 550 | 4600 |
| With Actuators | 1550 | 2050 |

Figure 5-9 shows the displacement plots of Rod4 for the machining conditions at 625 rpm with a depth of cut of 0.040 in (1.02 mm). Based on the results obtained from the experiments, the findings are summarized as follows:

1.    As power is supplied to drive the actuators, the tool tip initial equilibrium shifts inward towards the workpiece on average about 78.7 $\mu$in (2 $\mu$m) as

74

shown in Figure 5-10.

2.    Appropriate frequency and gain adjustment at which to drive the actuators
      are critical in achieving tool vibration compensation.  Improper adjustment
      leads to over compensation in which the tool tip has the capability to worsen
      rather than improve the surface quality.

3.    With appropriate frequency and gain adjustment, the actuators can be driven
      to yield a variation reduction of up to 10 percent.  Such result justifies the
      need to conduct an off-line optimization strategy to increase tool vibration
      control.
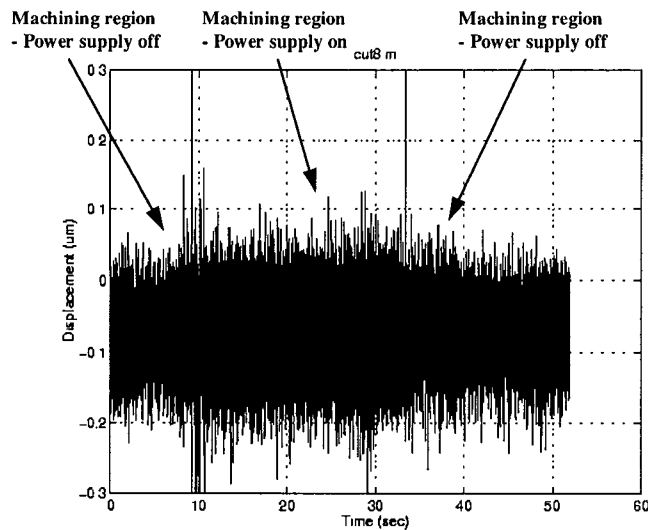


Figure 5-9 Displacement plots for identifying the optimal compensation
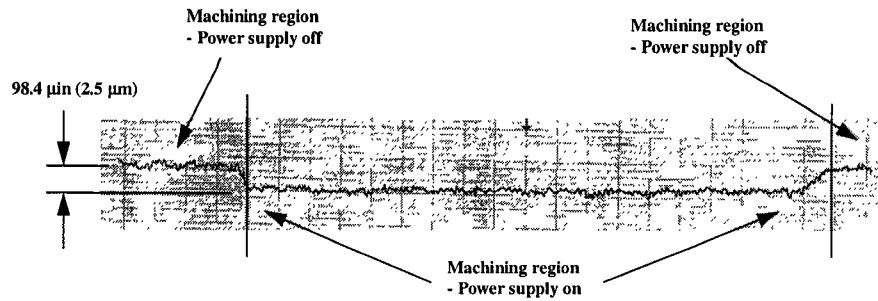
Figure 5-10  Surface profile of slot4_4 on Rod4


## 5.2.4   Experimental Set Four:  Phase-Shift Controller


In evaluating the phase-shift controller in compensating the vibration in the

shop floor environment, the displacement signal as measured from the VIT sensor is

used as the feedback signal to drive the actuators.  As described in Section 5.1.1, the

data acquisition system provides the capability of changing the time delay causing

the feedback signal to shift in the control loop.  The two variables of interest in

evaluating the performance of the phase-shift controller are the time delay in the

control loop and the gain amplitude.  As a result, the machining parameters used are

the same throughout the experiments except for the changes in the time delays and

the gain settings.  Based on the observations from previous experiments, the

selected machining conditions used were at 470 rpm, 0.040 in d.o.c. (1.02 mm), and

0.003 in/rev (0.08 mm).

Rod6 was machined.  Starting with the controller off, a small section was

machined.  The controller and the power supply to the actuators were then switched

76

on. The procedure was repeated for six times. The frequency to send to the controller from the computer was sent and the gain settings on the power supply was adjusted. The frequency sent to the controller was from 50, 150, ..., 300. By observing the vibration signal on the scope, the gain setting was set at the brink of oscillation. As soon as oscillation occurred, the gain was lowered. Throughout the experiments, the voltage across the actuators were measured to be less than 25 V rms. The phase shift angle associated with each frequency is given in Table 5-9.

Table 5-9 Relationship between phase shift angle and frequency

| Frequency (Hz) | Phase Shift (Degrees) |
|---|---|
| 50 | 161 |
| 100 | 130 |
| 150 | 99 |
| 200 | 69 |
| 250 | 38 |
| 300 | 7 |
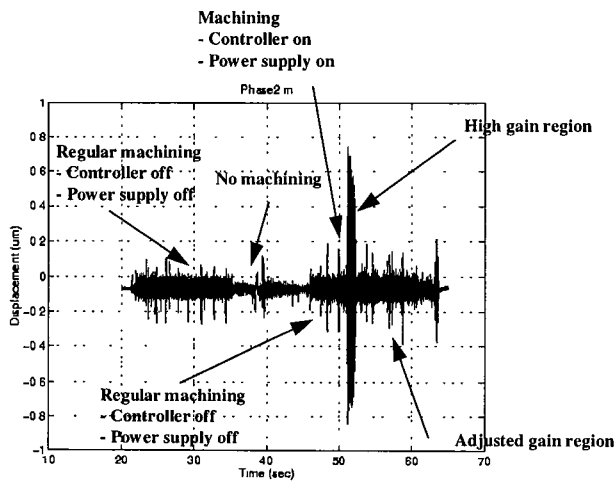


Figure 5-11 Typical displacement plot of the data collected

Machining
- Controller on
- Power supply on

Regular machining
- Controller off
- Power supply off
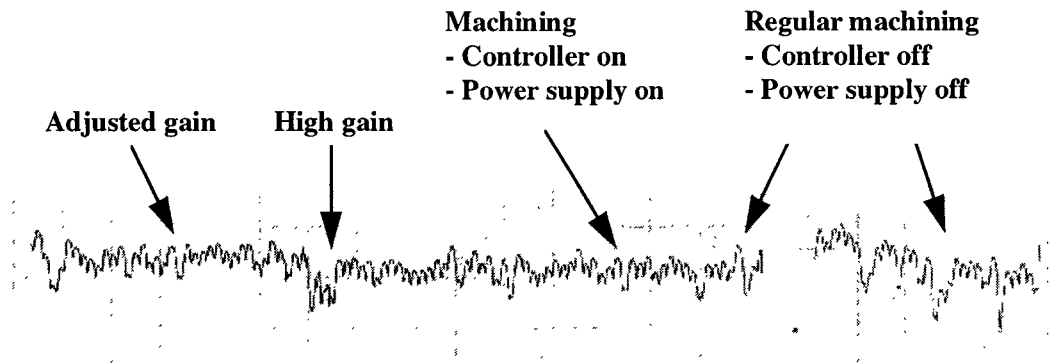
Adjusted gain          High gain

Figure 5-12  Surface profile of the machined region on Rod6

Figure 5-11 shows a typical displacement plot of the way data was collected

with the critical regions identified and labeled.  The controller was set at 50 Hz (or

shifted 161 degrees).  Figure 5-12 shows the surface profile of the workpiece of the

region.  The results obtained can be summarized as follows:

1.    Avoiding over compensation becomes increasingly critical with the use of

the phase-shift controller.  A slight increase in the gain can drastically over

compensate the tool vibration signal.  For effective vibration attenuation, the

gain must be adjusted at the point before over compensation occurs.

2.    Results show the phase-shift controller has the capability of attenuating the

vibration during machining provided that it can effectively control or limit

the gain at the onset of over compensation.  As a result, it is expected that

any general type of controller with the capability of automatically adapting to

the gain can attenuate the machining vibration using the current tool post

system.

# Chapter 6

# Conclusions and Recommendations

## 6.1   Conclusions

The work presented in this thesis represents a summary of the on-going research project -- using PMN actuators for vibration compensation during machining. The ultimate goal of the project is to apply electrostrictive material-made actuators to industrial applications with focus on machine tools. This thesis research characterizes the efforts in the third stage after the completion of the tool post structural design [17] and the feasibility study of using phase-shift concept for active vibration control [18]. The accomplished work of this thesis is summarized as follows:

1.    Development and construction of a stable and reliable testbed for testing dynamic behavior of the designed tool post structure has been a major contribution of this thesis research. At the time when the mechanical structural design was completed and a prototype of the tool post was successfully fabricated, the mechanism to test the fabricated tool post did not exist. In this thesis research, the experimental testbed was formulated under

a computer-controlled environment. The testbed environment consists of a sensing system, a data acquisition system, and a set of experimental apparatus and devices to monitor the excitation force and vibration characteristics as well as to record the experimental data. Efforts toward hardware realization and purchases of equipment have been one of the major challenges to complete the testbed. Not only have these efforts laid down the ground work for this thesis research, but also have provided valuable assistance to the research work conducted or to be conducted by the entire research team. The introduction of LabVIEW, an advanced programming software, has facilitated in computer simulation, data acquisition, and data analyses, serving as a unique example of the contributions made in this work.

2. As presented in this thesis, the third stage of the tool post project is characterized by identifying the performance of the tool post in terms of active vibration compensation. The work completed in this stage consists of:

(1) testing the tool post with no presence of actuators

(2) testing the tool post with the presence of actuators and with no power supply

(3) testing the tool post with the presence of actuators with power supply and with no controller involvement

(4) testing the tool post with the presence of a controller designed by Dold [18]

3.  Results obtained from this research strongly indicate that PMN actuators are

excellent candidates to be used for vibration control on machine tools.  The

significant findings of this research are:

(1)    Placement of actuators in the tool post structure increases the system

rigidity significantly.  In this research, with the placement of the

actuators, results have shown that the magnitude of displacement

from the VIT sensor decreases on an average by about 70 percent.

This indicates that the static stiffness of the designed tool post falls in

an appropriate region, in which a room has been reserved for the

PMN actuators to statically and dynamically adjust the system

rigidity for the purpose of vibration compensation.

(2)    The capability of PMN actuators to perform vibration compensation

can be quantitatively described by two parameters, namely, shift of

the tool tip equilibrium position and reduction of the variation of the

tool tip about the equilibrium position.  In this research, an average

of 2 $\mu$m for the equilibrium position shift and 10 percent of the

variation reduction have been observed.  These observations offer a

unique opportunity to carry out off-line optimization for tool

vibration control.

(3)    A designed controller, based on the concept of phase-shift for

vibration compensation, has been tested.  The obtained results have

indicated reduction of tool vibration during machining, and consequently, improvement of surface finish, showing great promising.

4.  There is a principal material property issue which remains as a barrier to system implementation of PMN-based actuators. The issue is the coupling coefficients, which serve as an indicator of the efficiency of conversion from electrical energy to mechanical energy and vice versa. At present, these coupling coefficients are between 0.3 and 0.45, depending on the operating conditions. They are relatively low. This fact has major system impact, affecting power suppliers, cabling, and handling systems, such as the designed tool post. In order to maintain an acceptable level of energy conversion, special attention has to be paid to

(1)  avoidance of over-compensation. Over-compensation introduces negative effects on controlling tool motion and represents a loss of energy for doing something unnecessary. Here frequency and voltage of the power amplifier are two key factors. Increase of the voltage level speeds up polarization and leads to an unnecessary large displacement for vibration compensation. On the other hand, as the driving frequency varies, the effective actuator impedance varies accordingly, leading to over-compensation.

(2)  Maintenance of a balance between the actuator impedance and the

current through actuator. A major contribution of this research is an introduction of an audio power amplifier. The biased DC voltage is set at 54 volts, and the control voltage is -25 to 79 volts. The actuator stroke level achievable is about 17 $\mu$m.

5.    Finite element method is an excellent tool to use for design analysis and design optimization in the mechanical structure of the smart tool post. Based on the study presented, the membrane components have performed their intended functions of allowing the actuators the authority to control the vibration. Predictions of the displacement and hence the stiffness of the membranes have agreed with experimental testing where FEM prediction has shown a 0.19 $\mu$m displacement as compared to 0.25 $\mu$m for a unit force application. Additionally, FEM has shown that the membrane components cannot buckle during machining.

## 6.2   Future Work

Significant progress has been made as presented in the present study. However, there are still many remaining technical areas that need to be continued and developed. Suggestions for future work are presented as follows:

1.    The use of finite element method in the design analysis can be extended much further by studying the static and dynamics behavior of the tool post as

a system. Through 3-D modeling and analysis, the interaction of the various components of the tool post acting as a system can offer a great insight into the mechanical response of the tool post. More importantly, the response can be visually displayed to observe how the mechanical structure shifted its equilibrium during the actual machining. With the testbed and the precision sensing system, the results from FEM can be verified and corrected through experimentation.

2. The off-line optimization strategy studied apply to only Aluminum 6061-T6 workpiece. Displacement measurement shows that the magnitude of vibration for aluminum is between 1 to 2 microns while the range of the VIT sensor is up to 25 microns. Additionally, the enhanced power amplification system is capable of generating a tremendous amount of actuating force onto the surface. As a result, it is of interest to subject the tool post to machine other materials such as steel or other advanced ceramics materials.

3. It has been shown that the phase-shift controller can be used for vibration compensation during machining. However, the controller itself has a very limited working bandwidth. Improvement on the controller can be made to increase its robustness and adaptiveness.

# Appendix A

# Data Acquisition System

## A.1 Overview of Data Acquisition System

The data acquisition system consists of a Pentium, 90 MHz personal computer, two plug-in boards, and a signal conditioning chassis with two modules. The two plug-in boards are the AT-MIO-16X (or MIO for short) and the Digital Signal Processing Board 2200 (DSP2200). As the name implied, the MIO board is a general purpose, 16-bit card with multiple inputs and multiple outputs capability. An external chassis is connected to the MIO card through a 50-pin ribbon cable. The DSP2200 is a high-end board with its own CPU and memory for intense computation purposes. The DSP2200 has two filtered analog input channels and two analog output channels.

The signal conditioning chassis has 4-slots to house four SCXI modules (Signal Conditioning Extensions for Instrumentation). The four modules can be the same or different depending upon the needs of the user. For the data acquisition system described above, two SCXI modules are used: the 1121 and the 1140. SCXI 1121 is a four channel inputs with isolation capable of providing current or

voltage source excitation. There is a built-in cold junction reference point as well as jumper configurations for making quarter-bridge or half-bridge connections. The SCXI 1121 is ideal for applications using thermocouples, thermistors, RTDs, and strain gages. The SCXI 1140, on the other hand, has eight simultaneous sampling channels with track and hold amplifiers. Each channel can be configured independently to a gain of 1, 10, 100, 200, or 500. For each SCXI module, different type of terminal blocks can be attached. The purpose of the terminal blocks is to facilitate wire hook-up as well as providing electronic shielding. For the data acquisition system, one terminal block the 1320 is attached to the SCXI 1121.

## A.2 Cable Hook-up for the Data Acquisition System

The first step in the data acquisition process is the connection of the sensor to the data acquisition card. The key factor in determining the type of connection to be made is dependent upon the type of signal coming into the DAQ card.

There are two types of signals: ground-referenced signal and floating signal. Ground-referenced signal refers to signal that is connected to the building ground at some point such as a plug-in function generator. The power to drive the function generator is from the wall outlet which is connected to the building ground. Floating signal, on the other hand, refers to signal that is not connected to the

86

building ground. Examples of floating signal are devices that are battery operated, thermocouples, and isolated signals.

After determining the type of signals, the MIO board must be configured to receive that type of signal. The configuration is to be done using WDAQCONF.EXE software in the window environment. No hardware configuration is needed, thus saving the user from having to pull the card out from the computer. The MIO board can be configured in three ways to collect the two types of signals: Referenced single-ended (RSE), non-referenced single-ended (NRSE), and differential (DIFF). The type of configuration used is depended upon the strength of the signal and the amount of signal conditioning required.

RSE is typically configured to use with floating signals such as those signals that came from battery-operated devices. RSE also recommended to be use when the signal voltage level is above 1 V. With RSE configuration, the MIO card reads its 16-channel inputs differently. That is, the positive end of the signal must be connected to one of the 16 positive input channels (ACH0 to ACH15). The negative end is connected to AI GND (analog input ground). It should be noted that ACH0 and ACH8 have the least amount of noise level compared to other channels since ACH0 and ACH8 are located closest to AI GND.

As mentioned above, floating signals typically means RSE configuration. This is because floating signal is not connected to a common ground point as the MIO card. The measured voltage is determined by measuring the potential

difference of the signal and multiplying the difference by the gain setting. By connecting the negative end of the signal to AI GND, the user is connected to the ground of the MIO card, which is connected to the ground of the PC, which is connected to the ground of the building. As a result, with a common ground point, there is no difference in the ground potential between the signal and card. Note that it is the potential difference in the ground potential that leads to error in measurement. If the signal from the sensor is expected to be less than 1 V, then DIFF configuration must be used. Details about DIFF configuration are described below.

NRSE is typically configured for ground-referenced signal. For this configuration, the positive end of the signal is connected to one of ACH0 to ACH1 but the negative end must be connected to the AI SENSE pin. The reason for using NRSE configuration is that different instruments exhibit slightly different ground level. With NRSE configuration, any potential difference between the MIO card and the signal ground appears as what is called a common-mode signal at the positive and negative inputs and this difference is rejected by the amplifier. Again, if the configuration is not determined correctly, the difference in ground potential will create errors in the reading.

DIFF configuration is a bit more involved since it can be used for ground-referenced signal as well as for floating signal. The primary reasons for using DIFF configuration are the input signals must be at low level (less than 1V) and the signal

leads travel through noisy environments. To wire the connection with DIFF configuration, the positive end of the signal must be connected to ACH0 to ACH7 and the negative end of the signal must be connected to ACH8 to ACH15. ACH0 corresponds to ACH8 and so on. In addition, the negative end of the signal must be connected to AI GND. This type of connection works well if the signal is DC-couple and the impedance in the signal is less than 100 ohm. If the impedance is high then a bias resistor must be connected between the negative end of the signal input to AI GND. For even better noise rejection, two bias resistors can be used. However, the magnitude of the source of the signal will be reduced thus creating about -1% of the gain error.

If the signal is AC-coupled, a DC path must be generated from both inputs to AI GND. Connect a bias resistor between the positive input and AI GND for low impedance signal. If the source has high impedance, then two bias resistors should be used, one at each of the inputs. The resistance in the resistors must be low enough not to create an additional load but small enough to create the offset. Recommended resistance value is between 100 kohm to 1 Mohm.

# Appendix B

# LabVIEW Program Coding

## B.1  LabVIEW Block Diagram

The following figures show the block diagram of the major LabVIEW programs used in this thesis.
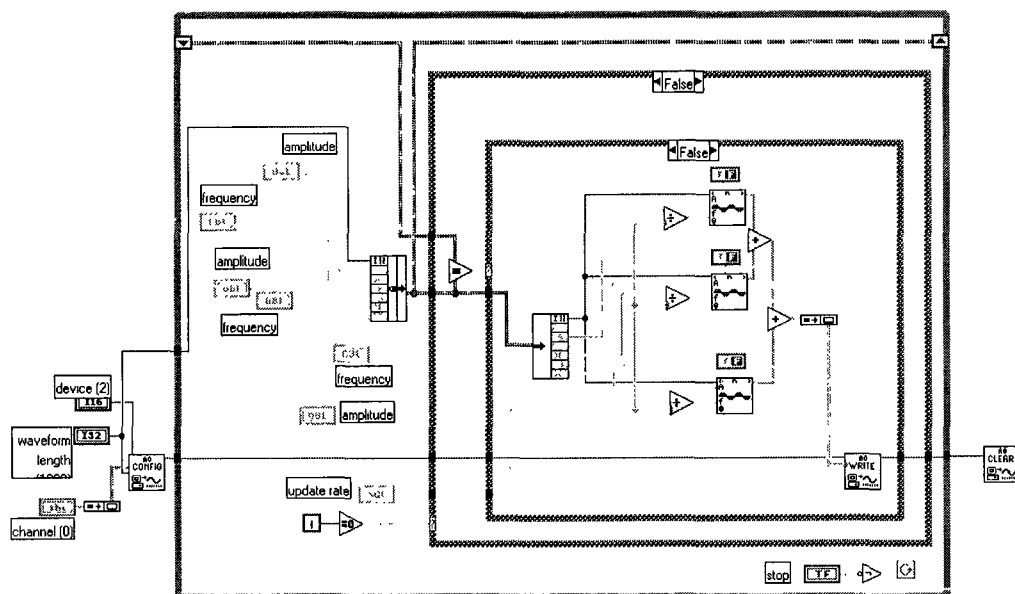


Figure B-1  Block diagram of the wave generator program
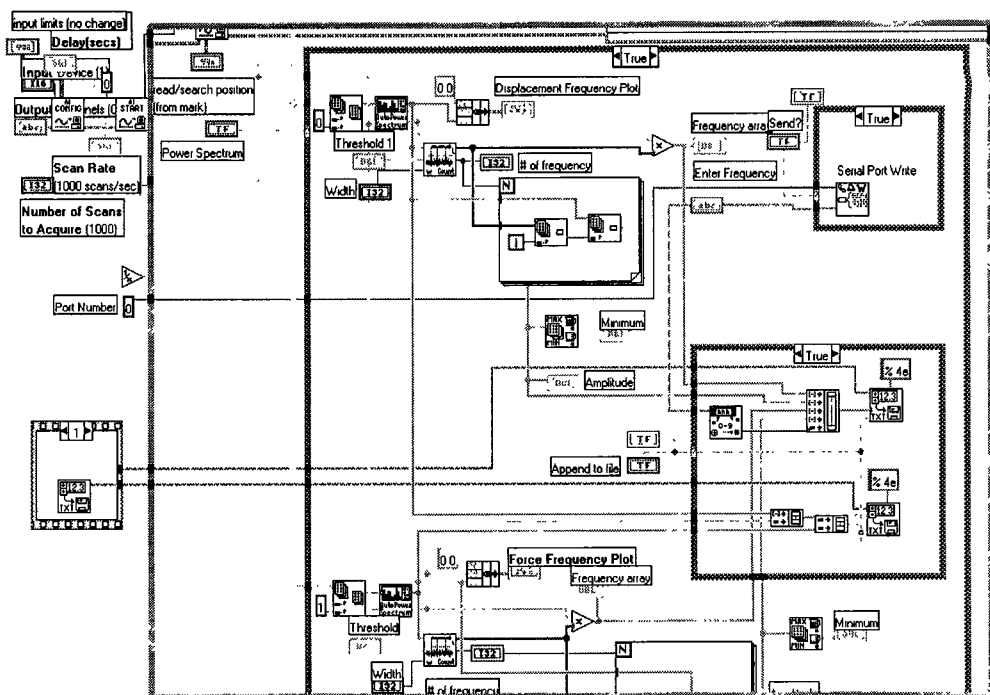
Figure B-2  Block diagram of detecting the linear spectrum peaks
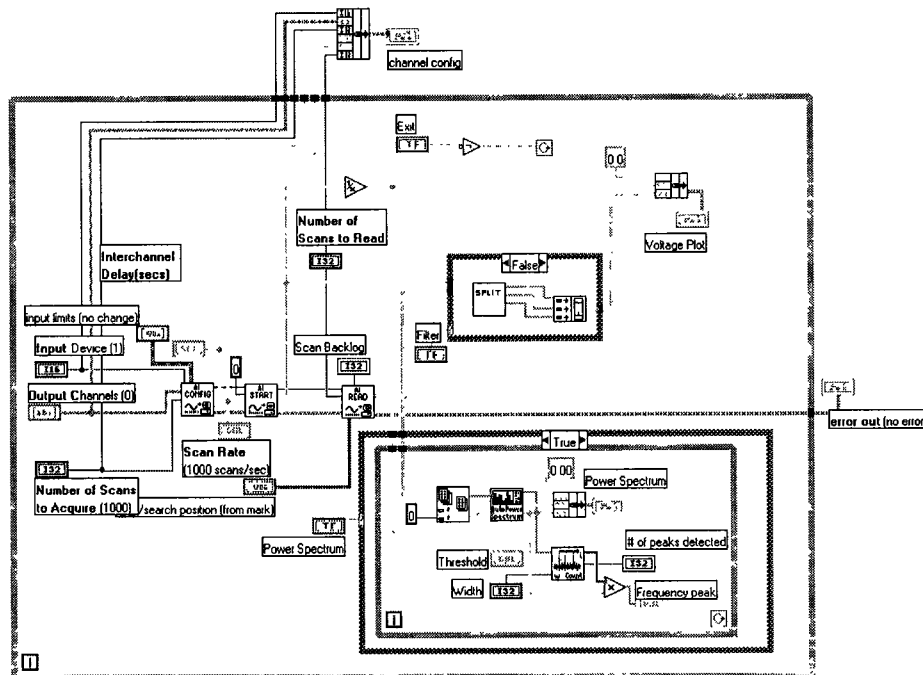


Figure B-3  Block diagram of the scope subprogram

91
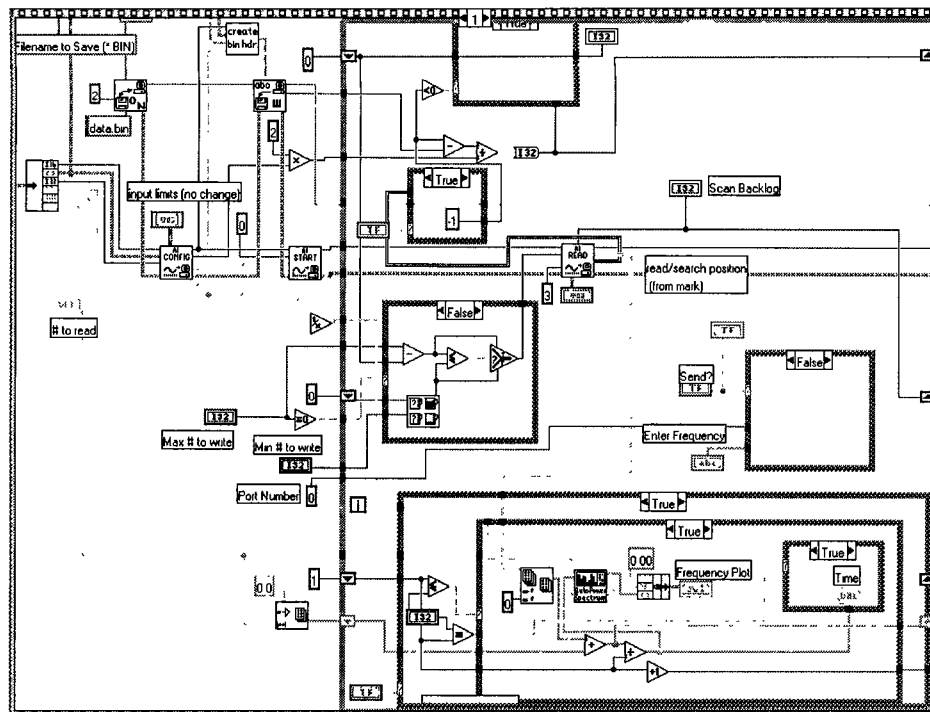
Figure B-4  Block diagram of the stream data subprogram
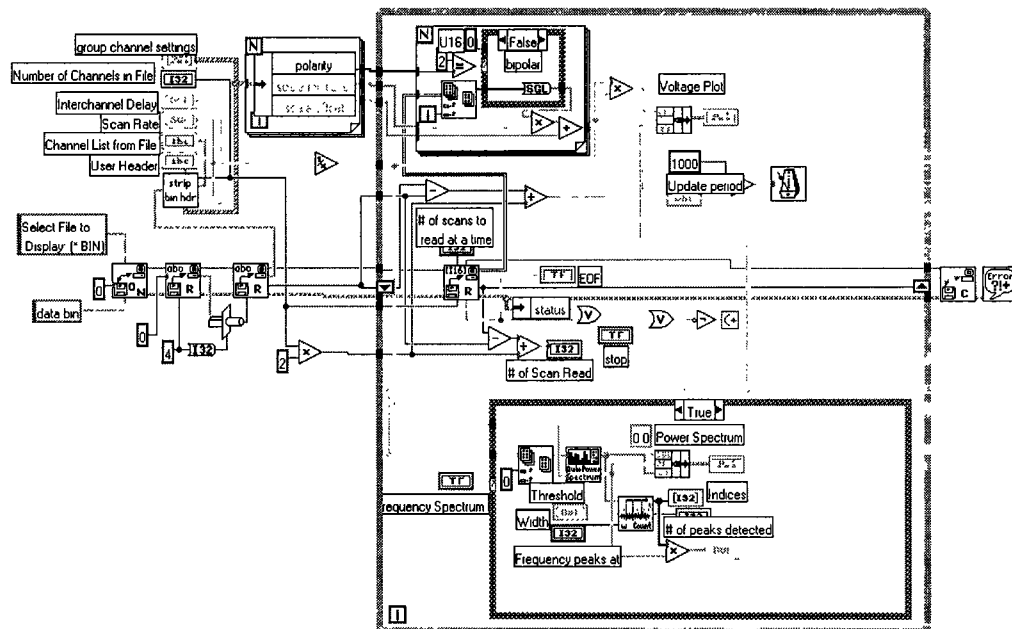
Figure B-5  Block diagram of the view data subprogram

## B.2 Other LabVIEW Programs Used

Other LabVIEW programs written and used in this thesis work are shown below. In Figure B-6, the program is written to facilitate the task of measuring the phase and amplitude difference between the force and acceleration signal used in characterizing the smart tool post structure. The program requires the user to input the path where two ASCII text files are located. When the two files are loaded, the user controls the frequency bandwidth in which to filter the signals. The program simply reads the cursor movement on the plots to calculate the phase and the amplitude difference in the signal.
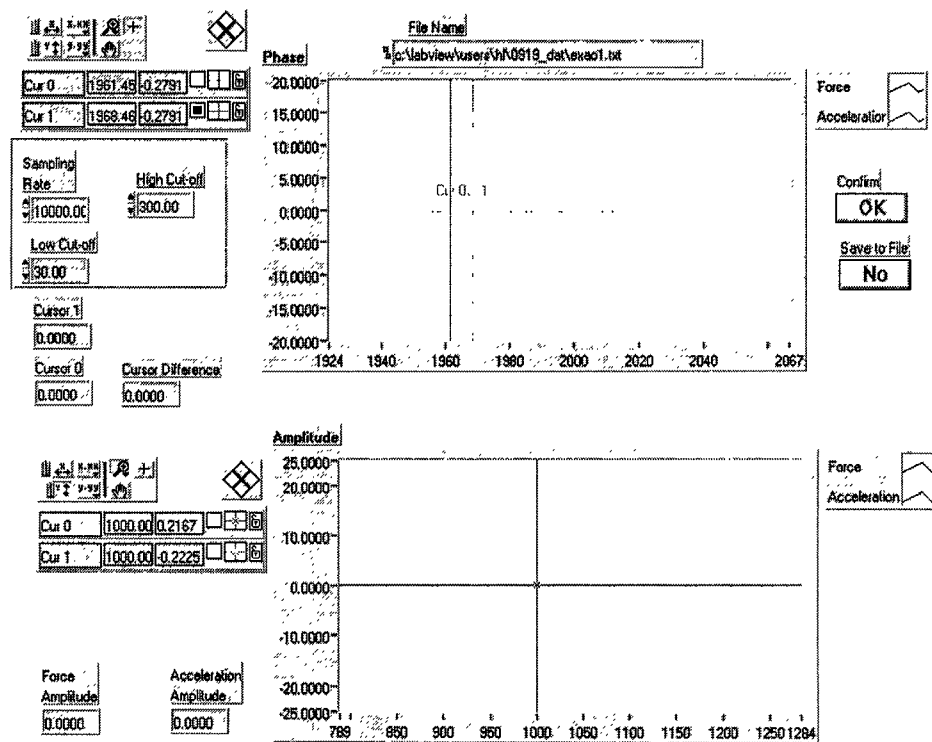


Figure B-6 Front panel of the phase and amplitude difference program
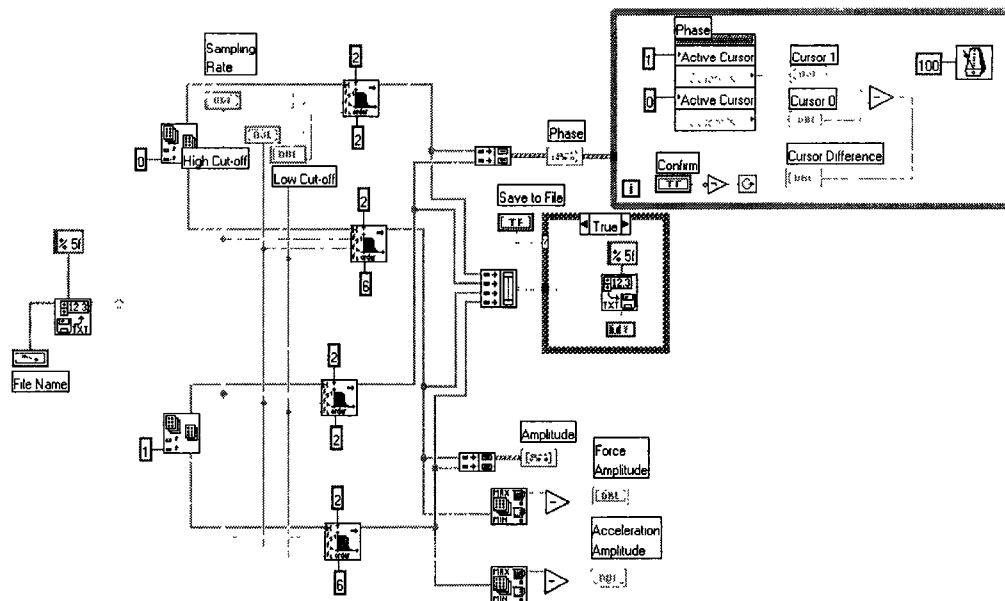
Figure B-7  Block diagram of the phase and amplitude difference program

Figure B-8 below shows a front panel of a frequency generator. In this program, different type of signals such as a sine wave, a square wave, and a sawtooth wave can be output. However, this program can only generate a signal with one frequency. As a result, this program is replaced with the three-frequency generator in conducting experiments on the tool post.

94

Figure B-8  Front panel of the frequency generator



Figure B-9  Block diagram of the frequency generator

95

# Appendix C

# Actuators Specifications

The following PMN actuator specifications are provided by AVX Corporation. Table C-1 presents the mean and the standard deviation of the capacitance and displacement measurements of PMN actuators. Figure C-1 shows the typical response curve of PMN actuators with respect to voltage, current, displacement, and the instantaneous power.

Table C-1  Capacitance and displacement specification of PMN actuators

| Test | Capacitance ($\mu$F) Mean | Std. Dev. | Displacement ($\mu$m) Mean | Std. Dev. |
|---|---|---|---|---|
| 1 | 3.9 | 0.05 | 17.1 | 0.19 |
| 2 | 4.4 | 0.02 | 17.1 | 0.03 |
| 3 | 4.4 | 0.07 | 17.5 | 0.20 |
| 4 | 4.3 | 0.08 | 17.2 | 0.28 |
| 5 | 4.5 | 0.06 | 17.2 | 0.49 |
| 6 | 4.4 | 0.13 | 17.0 | 0.28 |
| 7 | 4.5 | 0.13 | 18.5 | 0.02 |
| Average | 4.3 | 0.08 | 17.4 | 0.21 |

**Electrostrictive Response**



(a)

**Electrostrictive Response**
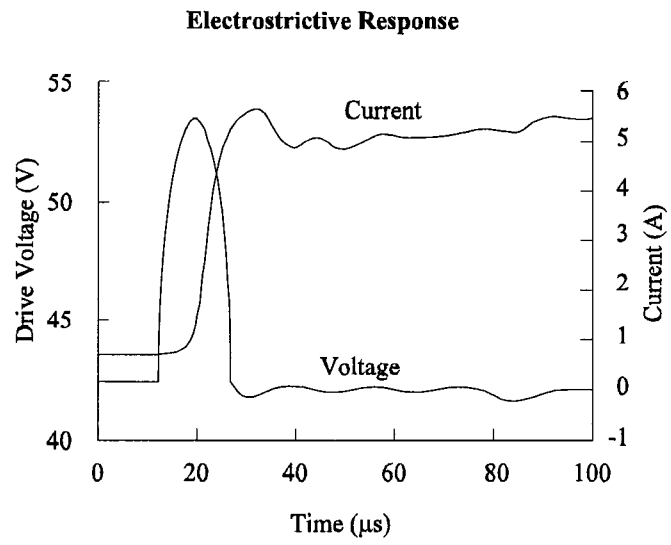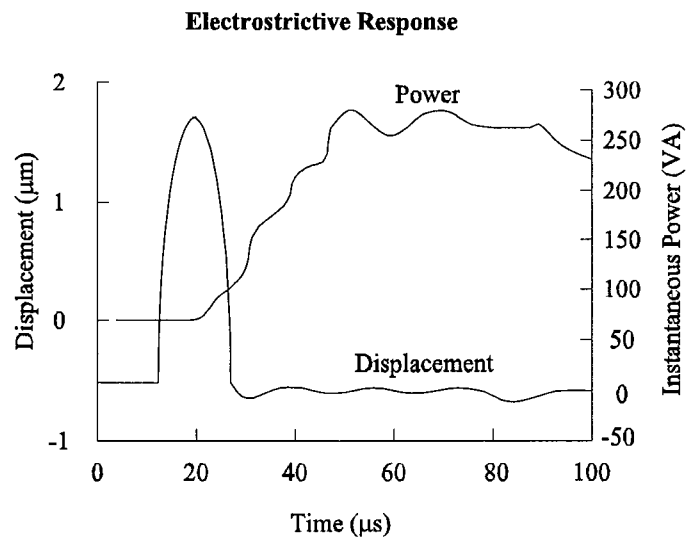


(b)

Figure C-1  Typical response curve of PMN actuators

97

# Appendix D

# Surface Measurement Data

## D.1 Displacement Plots

In this section, the displacement plots collected on the shop floor are presented. However, the number of plots is large. As a result, only randomly selected plots are pesented.



(a)                                  (b)
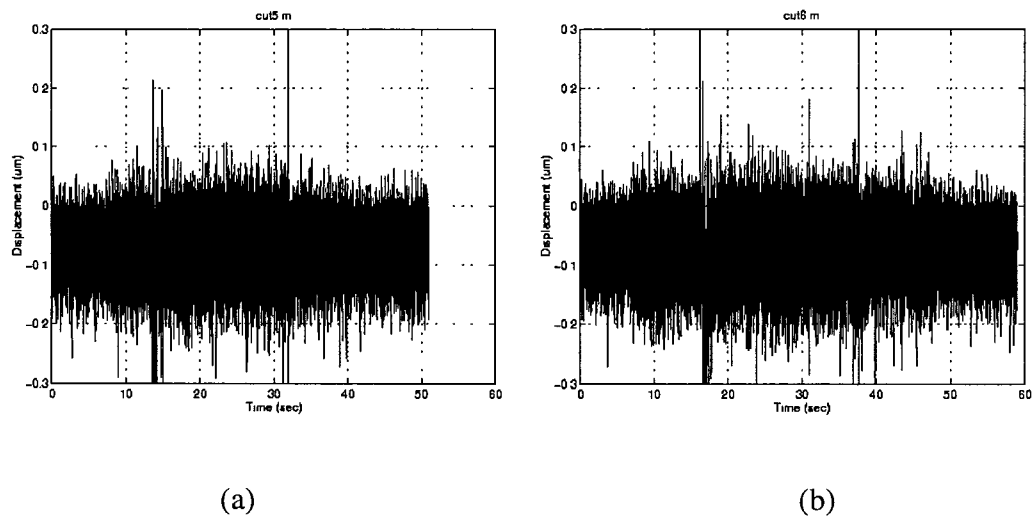
Figure D-1  Displacement plots of Rod4 experiments
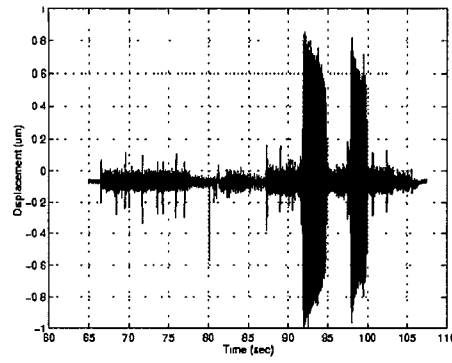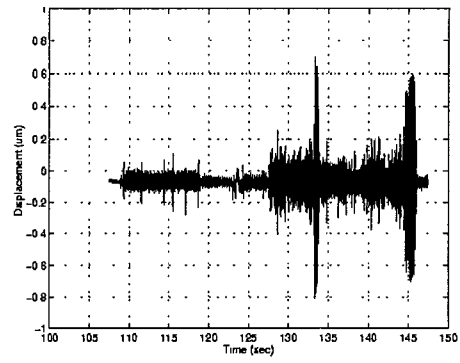
(a)                                    (b)
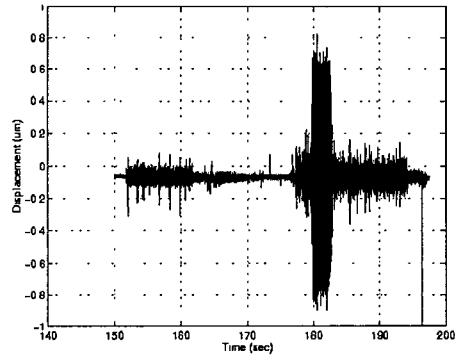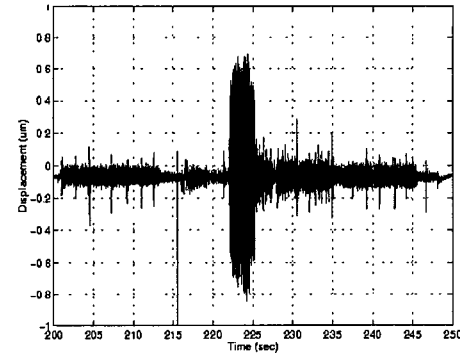
(c)                                    (d)

Figure D-2  Plots from the phase-shift experiments


## D.2  Surface Profile


The surface profile of the machined surfaces obtained from the frequency
and gain experiments are shown below.  Again, due to the page limitation, not all of
the surface profiles are included.
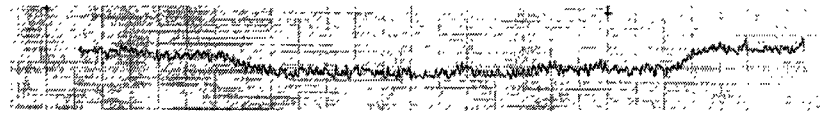
(a)  Slot 4_1
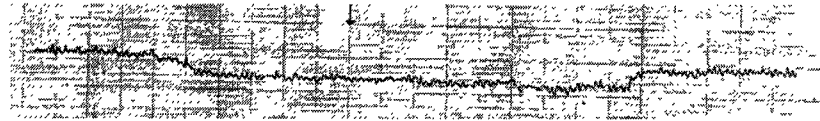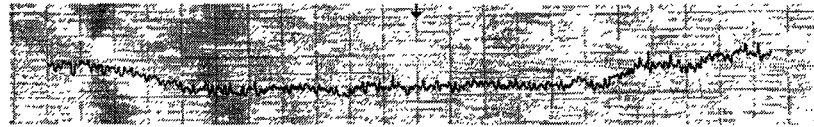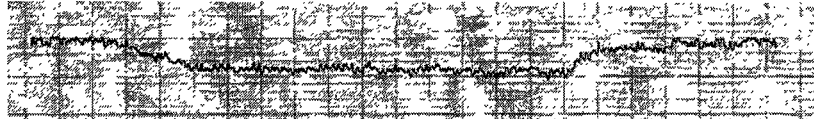
(b)  Slot 4_2
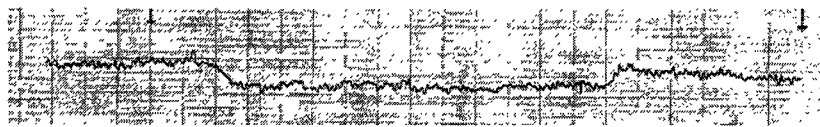
(c)  Slot 4_3
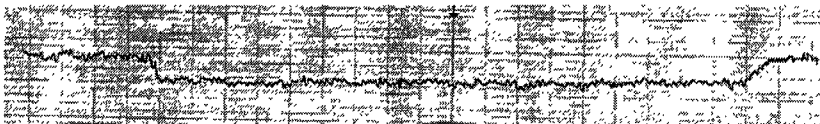
(d)  Slot 4-4
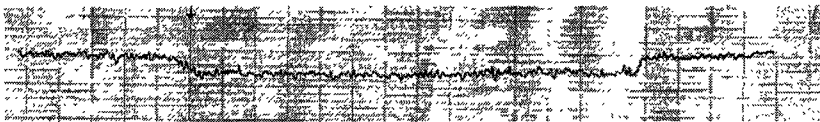
(e)  Slot 4_5
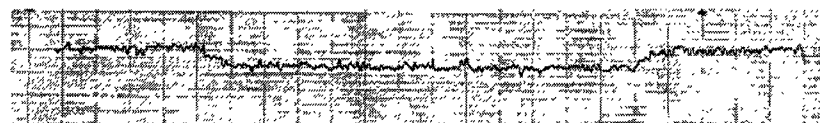
(f)  Slot 4_6

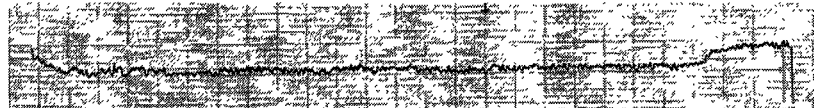Figure D-3  Surface profile of frequency and gain experiments at 0.04" d.o.c.

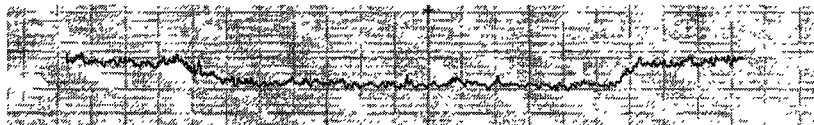(a)  Slot 5_1



(b)  Slot 5_2

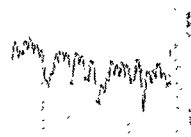

(c)  Slot 5_3



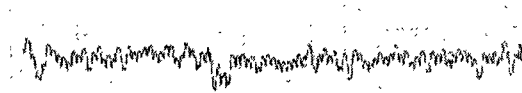(d)  Slot 5-4



(e)  Slot 5_5
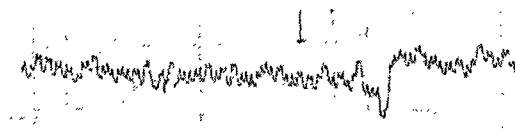


(f)  Slot 5_6

Figure D-4  Surface profile of frequency and gain experiments at 0.06" d.o.c.

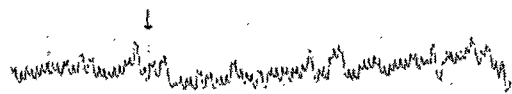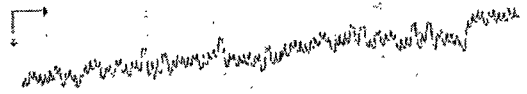(a)  Slot 6_1a

(b)  Slot 6_1b

(c)  Slot 6_2

(d)  Slot 6_3

(e)  Slot 6_4

(f)  Slot 6_5

Figure D-5  Surface profile of phase-shift controller experiments

# References

[1]     Losman, D. and Liang, S., <u>The Promise of American Industry:  An Alternative Assessment of Problems and Prospects</u>.  New York:  Quorum Books, 1990.

[2]     McClure, E., <u>The Competiveness Status of the U.S. Machine Tool Industry: A Study of the Influences of Technology in Determining International Industrial Competitive Advantage</u>.  Washington, D.C.:  National Academy Press, 1983.

[3]     "The SMS Partnership for Synthesis and Processing of Smart Materials: Final Program Review." Lockheed Martin, 1995.

[4]     <u>How to Run a Lathe</u>, 56th ed., Indiana:  South Bend Lathe, 1966.

[5]     <u>Clausing Colchester 15" Lathe Instruction and Parts Manual</u>.  Colchester: Colchester Lathe Company, Inc.

[6]     <u>How to Run a Lathe</u>, ibid.

[7]     Shaw, M., <u>Metal Cutting Principles</u>.  New York:  Oxford University Press, 1984.

[8]     Merritt, H. E., "Theory of Self-Excited Machine-Tool Chatter."  Journal of Engineering for Industry, November 1965, pp. 447-454.

[9]     Shaw, M., ibid, pp. 18.

[10]    Shaw, M., ibid., pp. 38.

[11]    Shaw, M., ibid, pp. 21

[12]    Welbourn, D. and Smith J., Machine-tool Dynamics:   An Introduction. Cambridge:  The University Press, 1970.

[13]    Spur, G, Schwermer, U., and Schule, A., "Model for Computing Quasi-static and Dynamic Displacements of Turning Centers." The American Society of Mechanical Engineers. PED-Vol. 45, 1990.

[14]    Manual of Lathe Operation and Machinists Table.    Michigan:    Clausing Corporation, 1971.

[15]    Welbourn, D., ibid.

[16]    Ulbrich, H. and Althaus, J., "Actuator Design for Rotor Control." The American Society of Mechanical Engineers. PED-Vol. 45, 1990, pp. 17-22.

[17]    Ko, Wing, Master Thesis:  A Systems Engineering Approach to Design a Smart Tool Post Structure.  University of Maryland at College Park, 1995.

[18]    Dold, George, Master Thesis:  Design of a Microprocessor-Based Adaptive Control System for Active Vibration Compensation Using PMN Actuators. University of Maryland at College Park, 1996.

[19]    Ashley, Steven, ed., "Rapid Prototyping is Coming of Age." Mechanical Engineering, July 1995, pp. 62-68.

[20]    Trent, E. M., Metal Cutting, 3rd ed., Oxford:   Butterworth-Heinemann Limited, 1991.

[21]     Black, Paul, <u>Theory of Metal Cutting</u>, New York:   McGraw-Hill Book Company, Inc., 1961.

[22]     Beards, C., <u>Vibration Analysis and Control System Dynamics</u>, New York: John Wiley & Sons, 1981.

[23]     Silva, Clarence, <u>Control Sensors and Actuators</u>, New Jersey:   Pentice Hall, 1989.

[24]     Gabel, Robert and Roberts, Richard, <u>Signals and Linear Systems</u>, 2nd ed., New York: John Wiley and Sons, Inc., 1980.

[25]     Ferreira, P., Kapoor, S., and Wang, A.   "Modeling of Machine Tools: Accuracy, Dynamics, and Control", PED-Vol. 45, New York:    The American Society of Mechanical Engineers, 1990.

[26]     Wei, B. and Rajurkar, P.   "Accuracy and Dynamics of 3-Dimensional Numerical Control Electrochemical Machining (NC-ECM)", PED-Vol. 45, New York: The American Society of Mechanical Engineers, 1990.

[27]     Eveleigh, Virgil, <u>Introduction to Control Systems Design</u>, New York: McGraw-Hill Book Company, 1972.

[28]     Rong, Yiming, Zhu, Yaoxiang, Zhang, Qicheng. "Development of a Micro-positioning system for Ultra-precision machines", PED-Vol. 45, New York: The American Society of Mechanical Engineers, 1990.

[29]     Paul, C., Nasar, S., and Unnewehr, L., <u>Introduction to Electrical Engineering</u>, New York:  McGraw-Hill Book Company, 1986.

[30] Zhang, G., Ko, W., Luu, H., and Wang, X.J., "Design of a Smart Tool Post for Precision Machining," Proceedings of the 27th CIRP International Seminar on Manufacturing Systems, May 1995, p. 157-164.